Preliminary results from SuperBIT

Ajay Gill

Postdoctoral Research Associate

MIT Department of Aeronautics and Astronautics

STAR Lab (Prof. Kerri Cahoy)

MIT AEROASTRO

Superpressure Balloon Borne Telescope (SuperBIT)

On the launch pad at Wanaka airport, New Zealand (credit: NASA / Bill Rodman)

Weak gravitational lensing

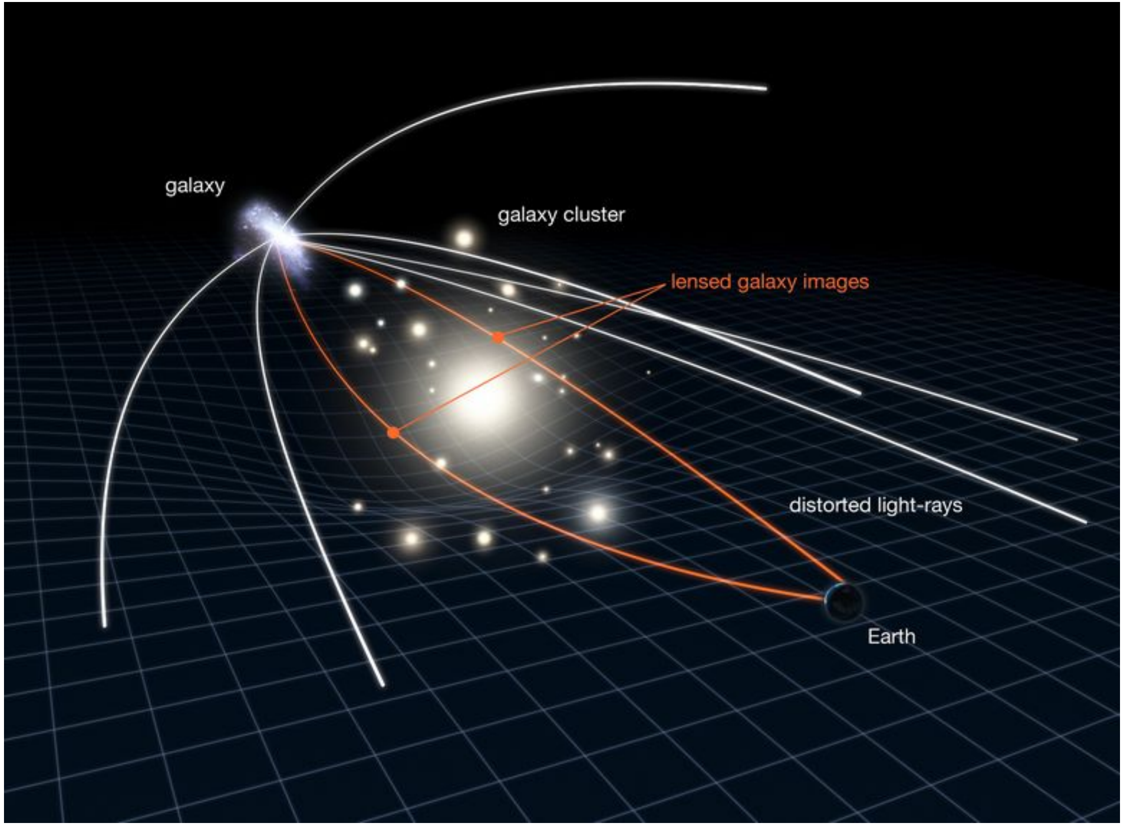

Credit: NASA/ESA

Ballooning

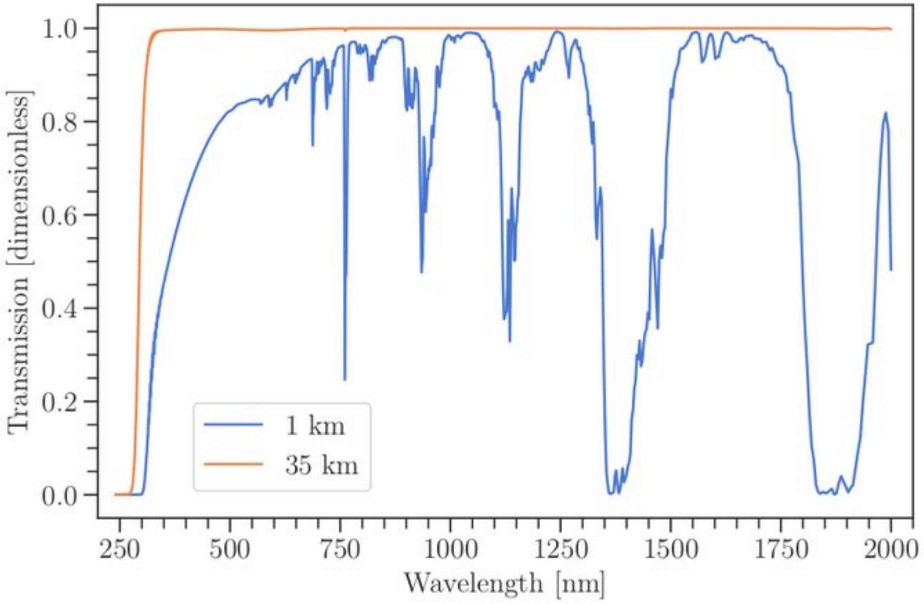

Seeing

Ground

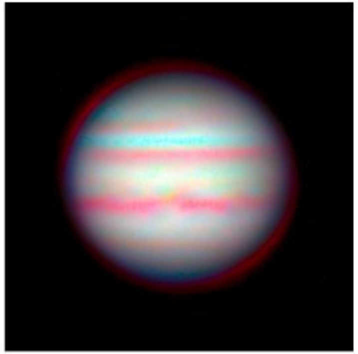

Float

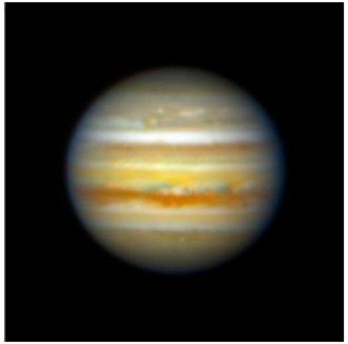

Backgrounds

See: *“**Optical Night Sky Brightness Measurements from the Stratosphere**”,*
Gill et al. (2020), AJ, Vol 16, arxiv:2010.05145

SuperBIT

- 0.5 meter diameter, f/11
- 0.37° x 0.25° field of view
  - ~ 30 times HST ACS
- Diffraction-limited imaging
  - PSF FWHM ~ 0.35″
- Science bands
  - *u, b, g*
- Typical exposure time
  - 5 minutes
- Science camera
  - **Sony IMX 455**

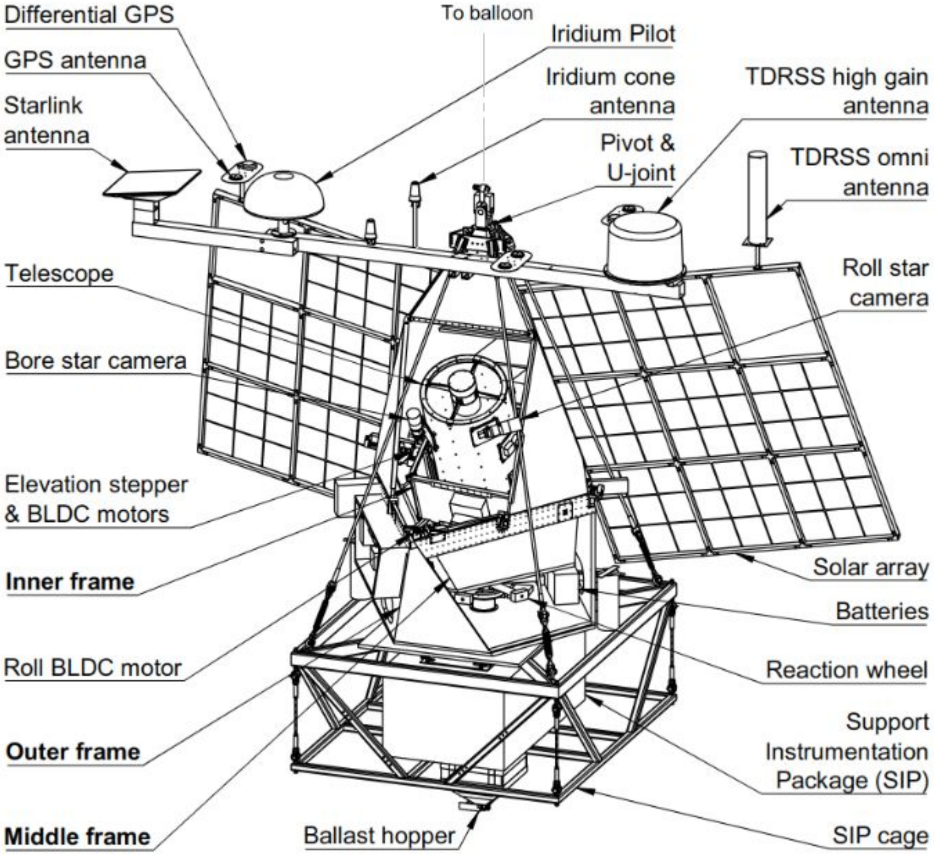

Gill et al. (2024) (submitted)

PRINCETON UNIVERSITY UNIVERSITY OF TORONTO JPL Jet Propulsion Laboratory California Institute of Technology Durham University MIT

SuperBIT systems

- Attitude determination and control system
- Optical system
- Detector system
- Thermal system
- Power system
- Communications system
- Autonomous operations system

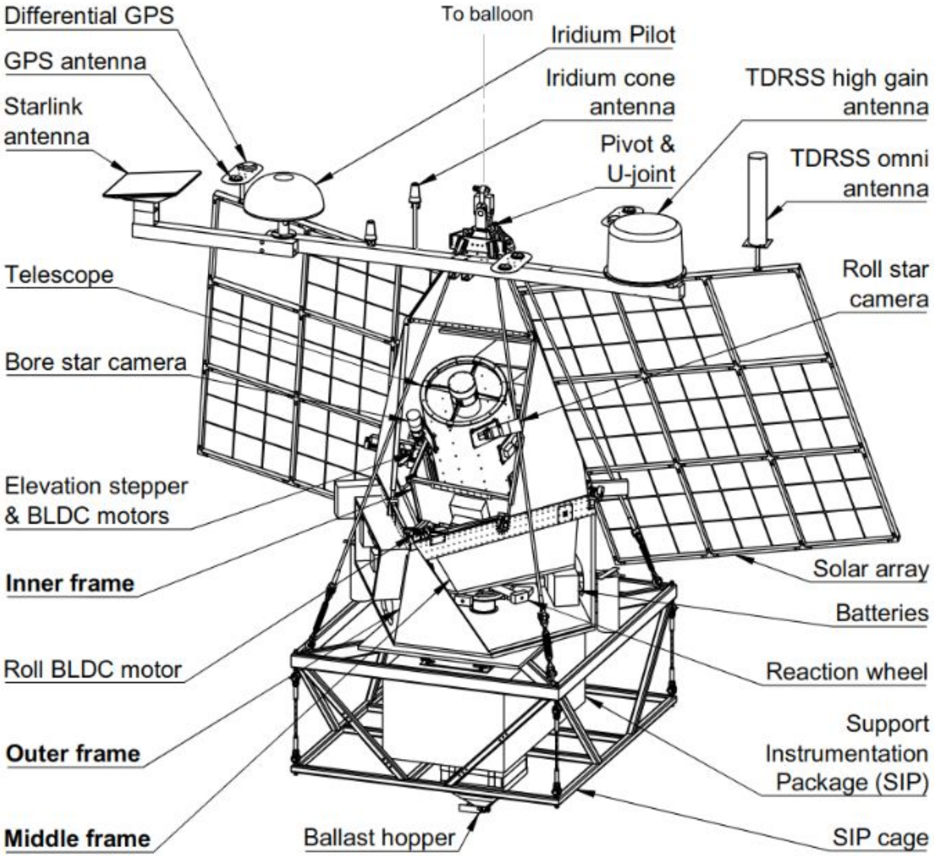

Gill et al. (2024) (submitted)

Attitude determination and control system (ADCS)

Credit: GIPHY

Attitude determination and control system

Step 1: Telescope stabilization (~ 0.3″)

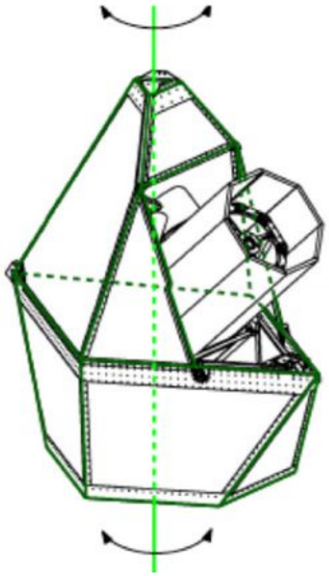

Yaw (0° – 360°)

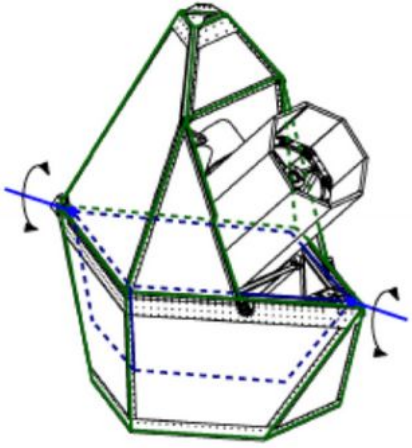

Roll (-6° – 6°)

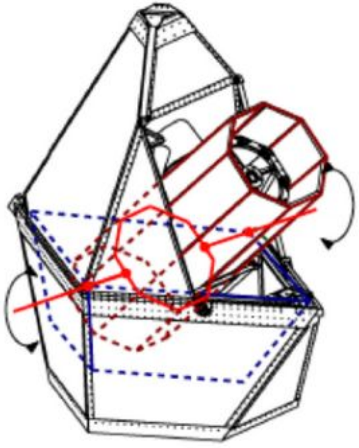

Pitch (20° – 60°)

Attitude determination and control system

Step 1: Telescope stabilization (~ 0.3″): **star cameras**

Camera	Basler acA2440-20gm
Sensor	Sony IMX264 CMOS
Lens	EF 300 mm f/4L USM
Lens adapter	ASCOM
Sensor size	8.4 mm × 7.1 mm
Sensor size	2448 pixel × 2048 pixel
Pixel size	3.45 μm × 3.45 μm
Plate scale	$2.37''$ per pixel
Read noise	2 e^-
Frame rate	23 fps
Interface	Gigabit Ethernet
Full-well capacity	11,000 e^-
Shutter	Global
Quantum efficiency	62% peak
Field-of-view	2.2 deg^2

Attitude determination and control system

Step 2: Image stabilization (~ **0.05″**)

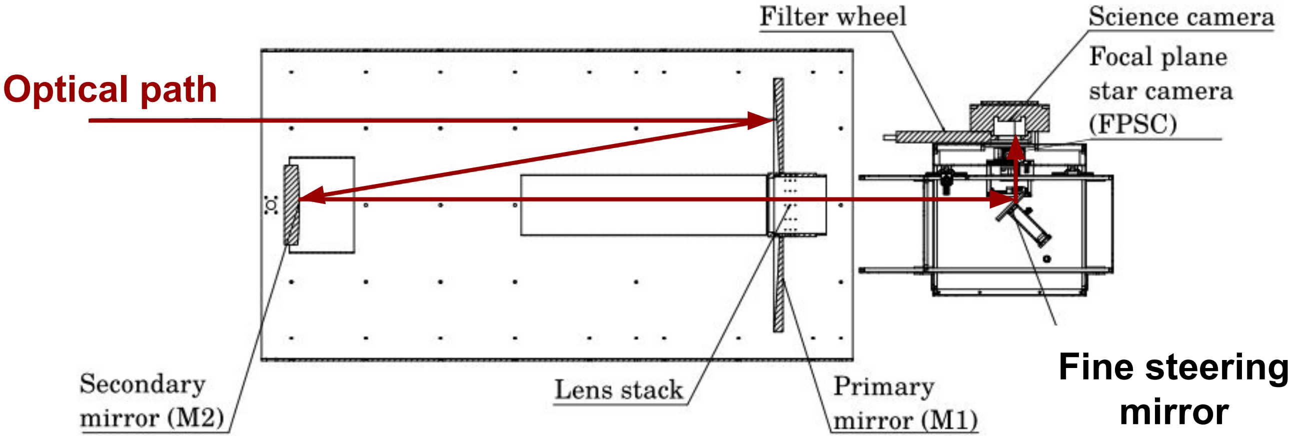

Attitude determination and control system

Step 2: Image stabilization (~ 0.05″): **star cameras**

Camera	Raptor Photonics KF674-CL	Basler daA1920-160um
Sensor	Sony ICX-674	Sony IMX-392
Sensor size	1940 pixels × 1460 pixels	1920 pixels × 1200 pixels
Sensor size	8.81 mm × 6.63 mm	6.6 mm × 4.2 mm
Pixel size	4.54 μm × 4.54 μm	3.45 μm × 3.45 μm
Plate scale	0.17″ per pixel	0.13″ per pixel
Read noise	7 e^-	2 e^-
Frame rate	6.2 fps	160 fps
Interface	Cameralink	USB 3.0
Full-well capacity	14000 e^-	9000 e^-
Shutter	Global	Global
Quantum efficiency	75% peak	60% peak
Field-of-view	0.006 deg^2	0.003 deg^2

Low-cost sensor characterization system

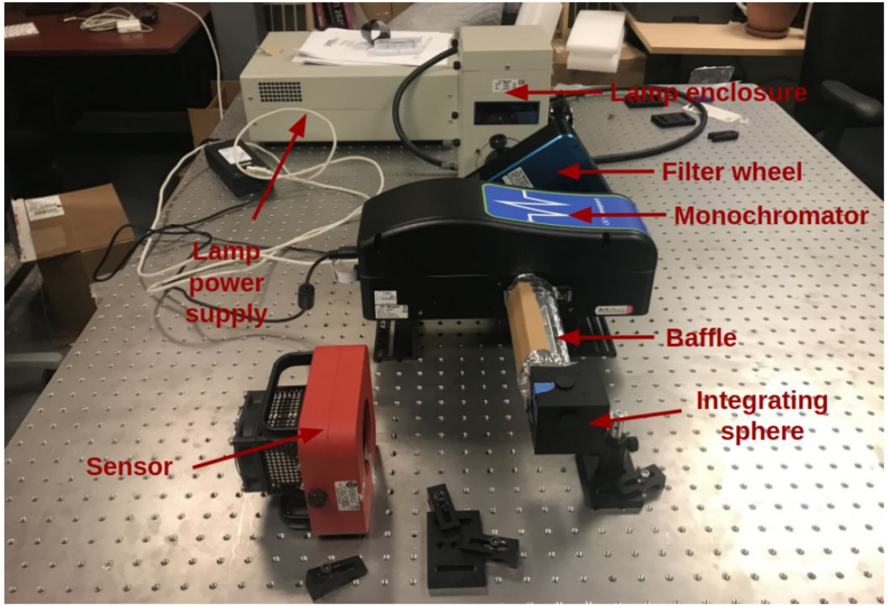

For full procedure, list of equipment, costs, see*: "**A low-cost ultraviolet-to-infrared absolute quantum efficiency characterization system of detectors",** Gill et al. (2022), SPIE, arxiv:2207.13052*

Xenon Arc Lamp, Newport, PN: 6258, $750

Credit: Newport

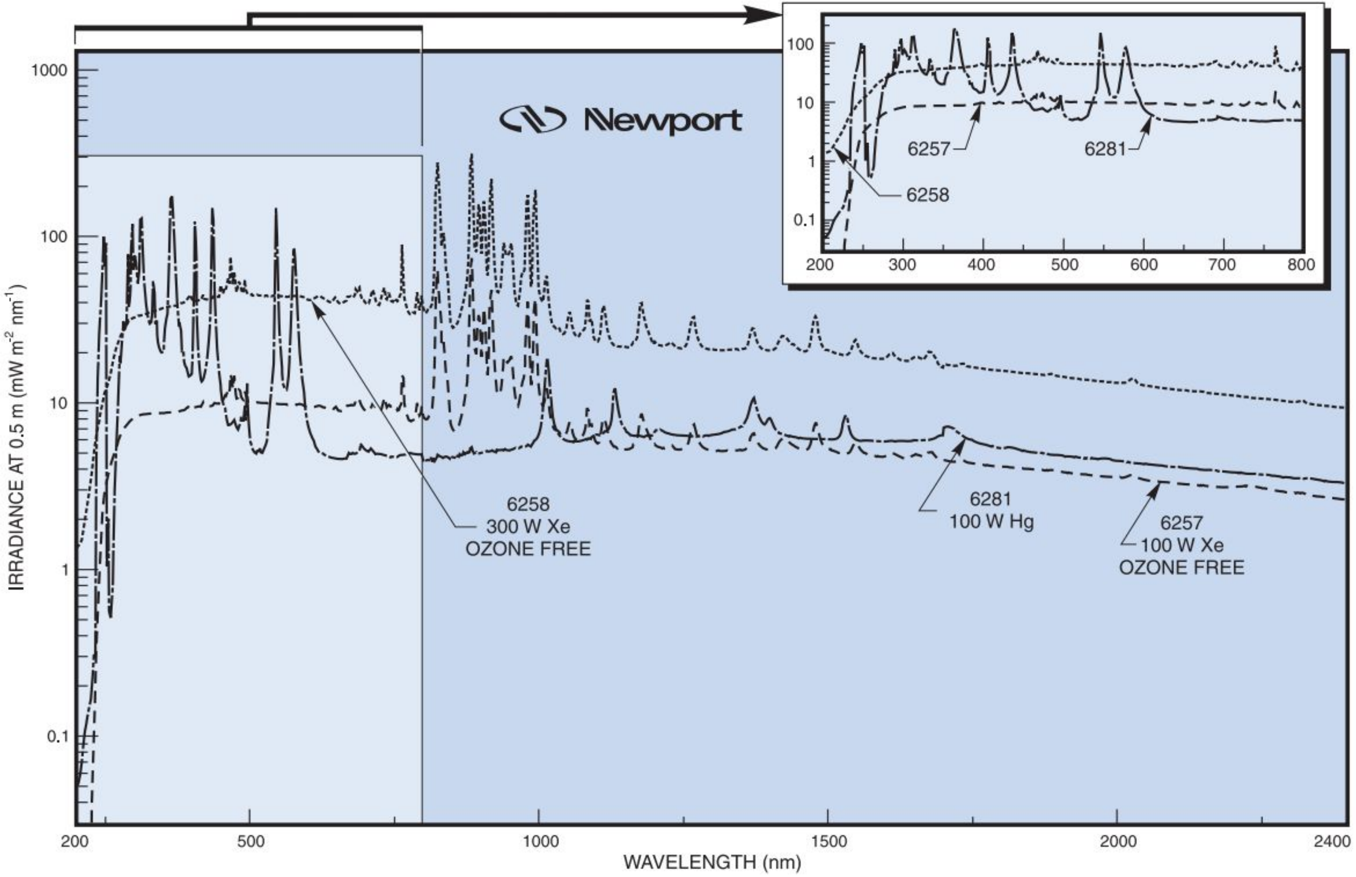

Credit: Newport

Power supply, Newport, PN: 69911, $5898

Credit: Newport

Monochromator, Newport, PN: CS130B, $7500

Credit: Newport

Integrating Sphere: Thorlabs, PN: IS200, 4-port 2", $1158

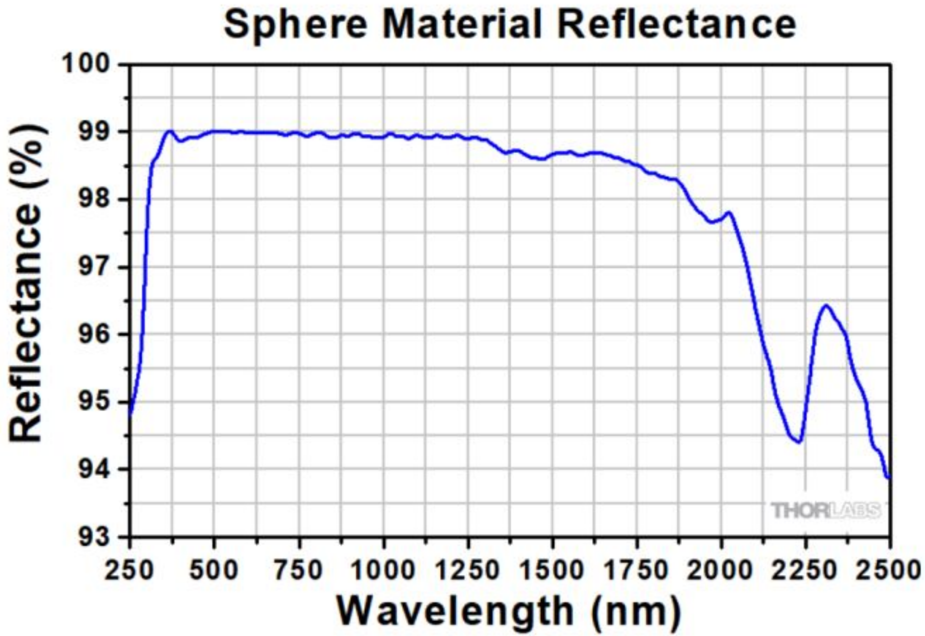

Credit: Thorlabs

Calibrated photodiode: Thorlabs, PN: S130VC, $670

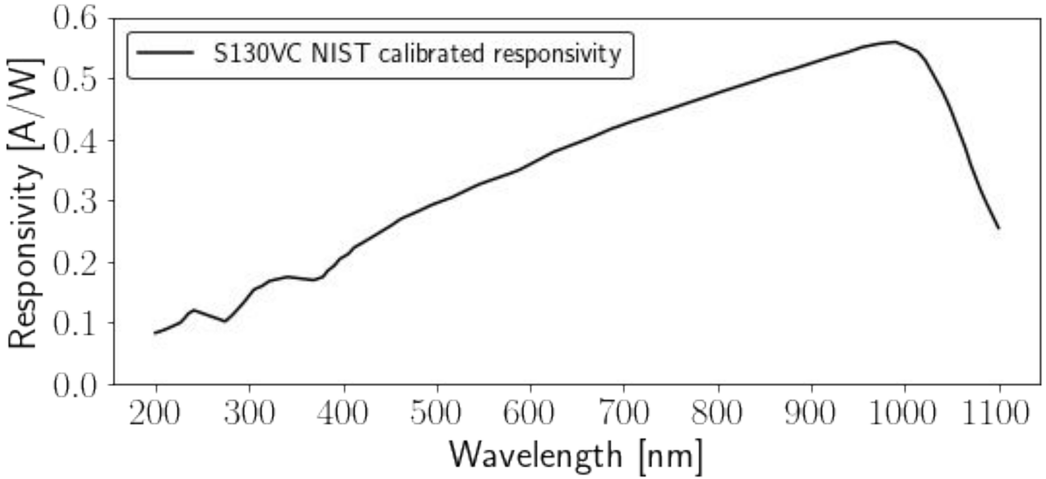

Credit: Thorlabs

Camera: QHY600

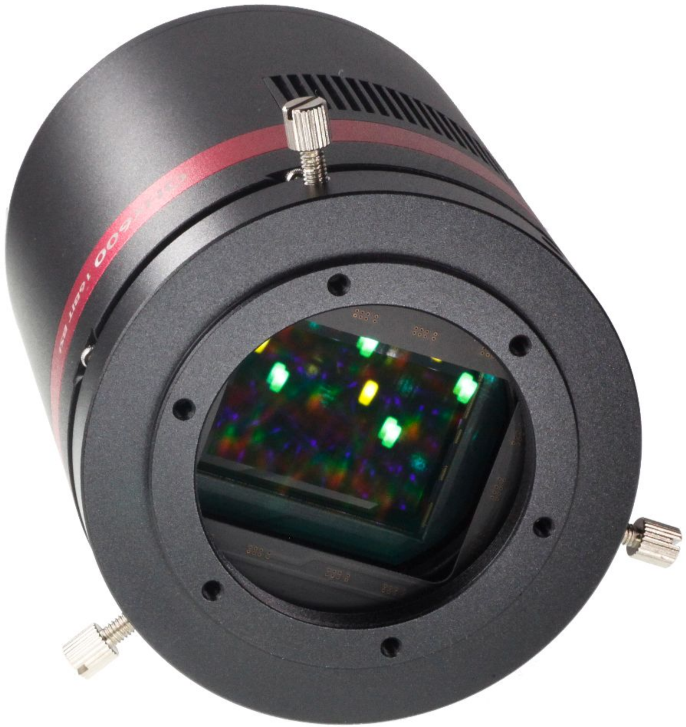

- Sensor: Sony IMX 455 BSI
- Pixel size: 3.76 um x 3.76 um
- Plate scale: 0.148" / pixel
- Sensor size: 36 mm x 24 mm
- Pixel array: 9576 x 6388
- Read noise: ~ 2 e- / pixel
- Full well: ~ 22,000 e-
- Dark current:
  - ~ 0.0035 e-/s/pixel at -10 C

Credit: QHYCCD

Sony IMX 455 Photon Transfer Curve

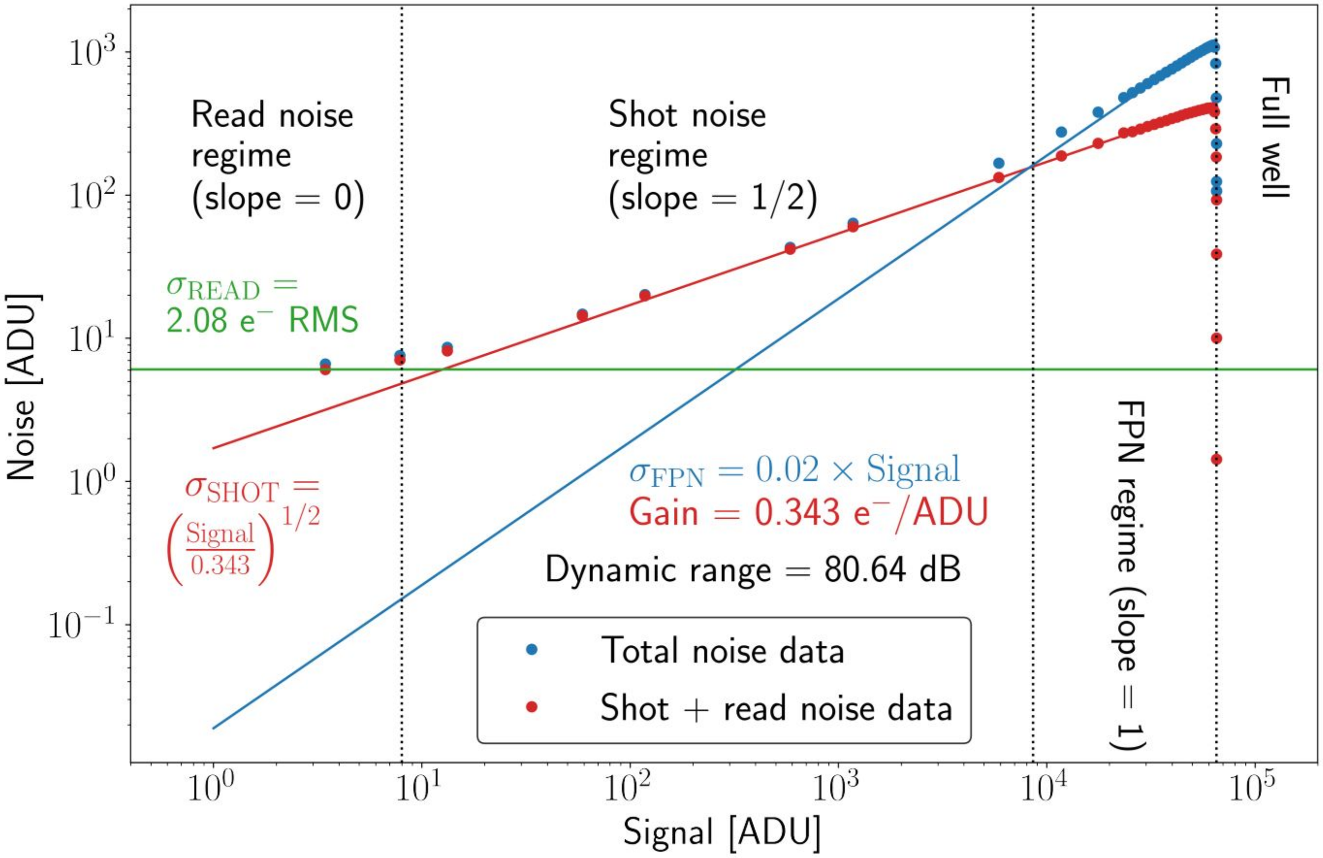

Gill et al. (2022), SPIE, arxiv:2207.13052

Sensor characterization: quantum efficiency

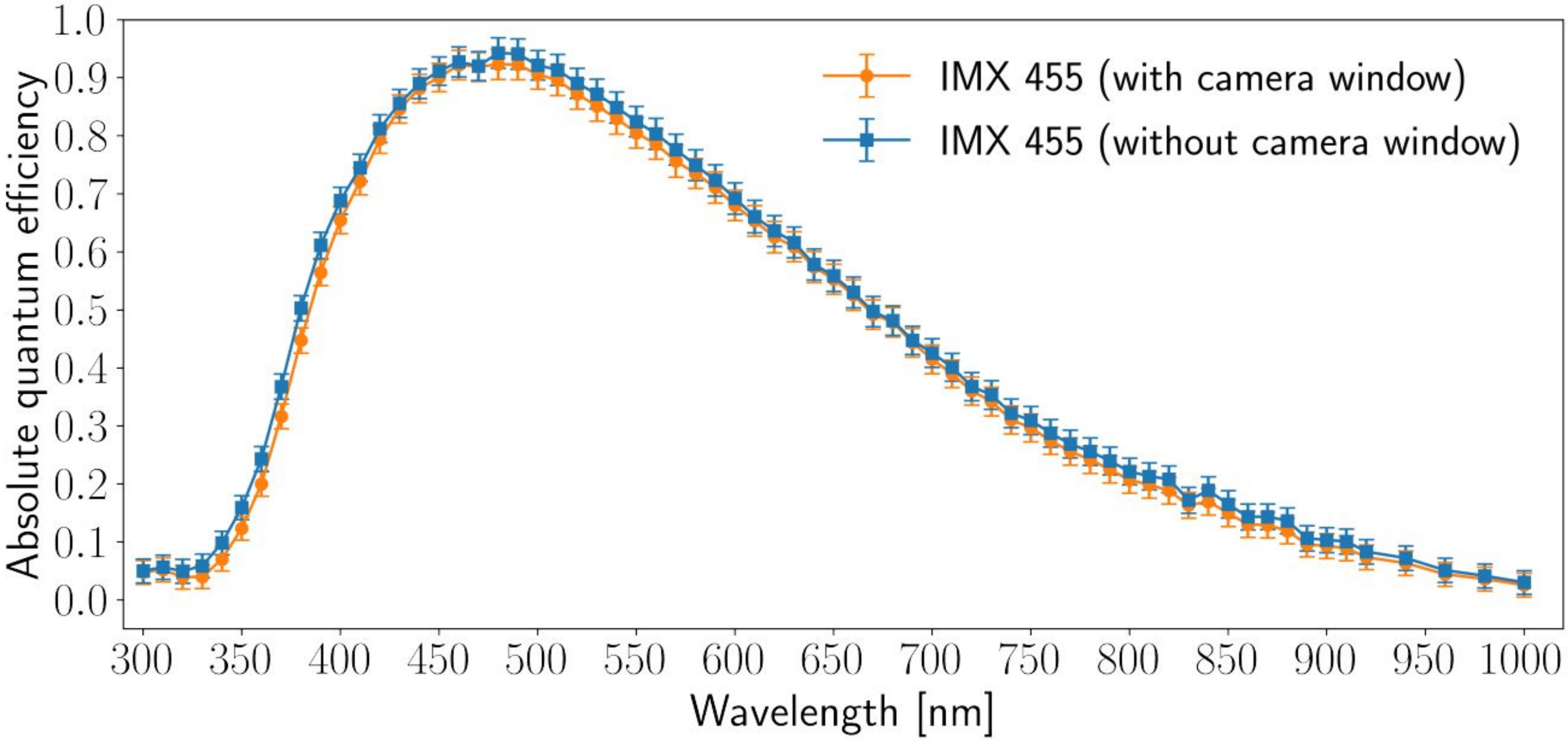

Gill et al. (2022), SPIE, arxiv:2207.13052

Quantum efficiency transfer curve: GSENSE 2020 BSI

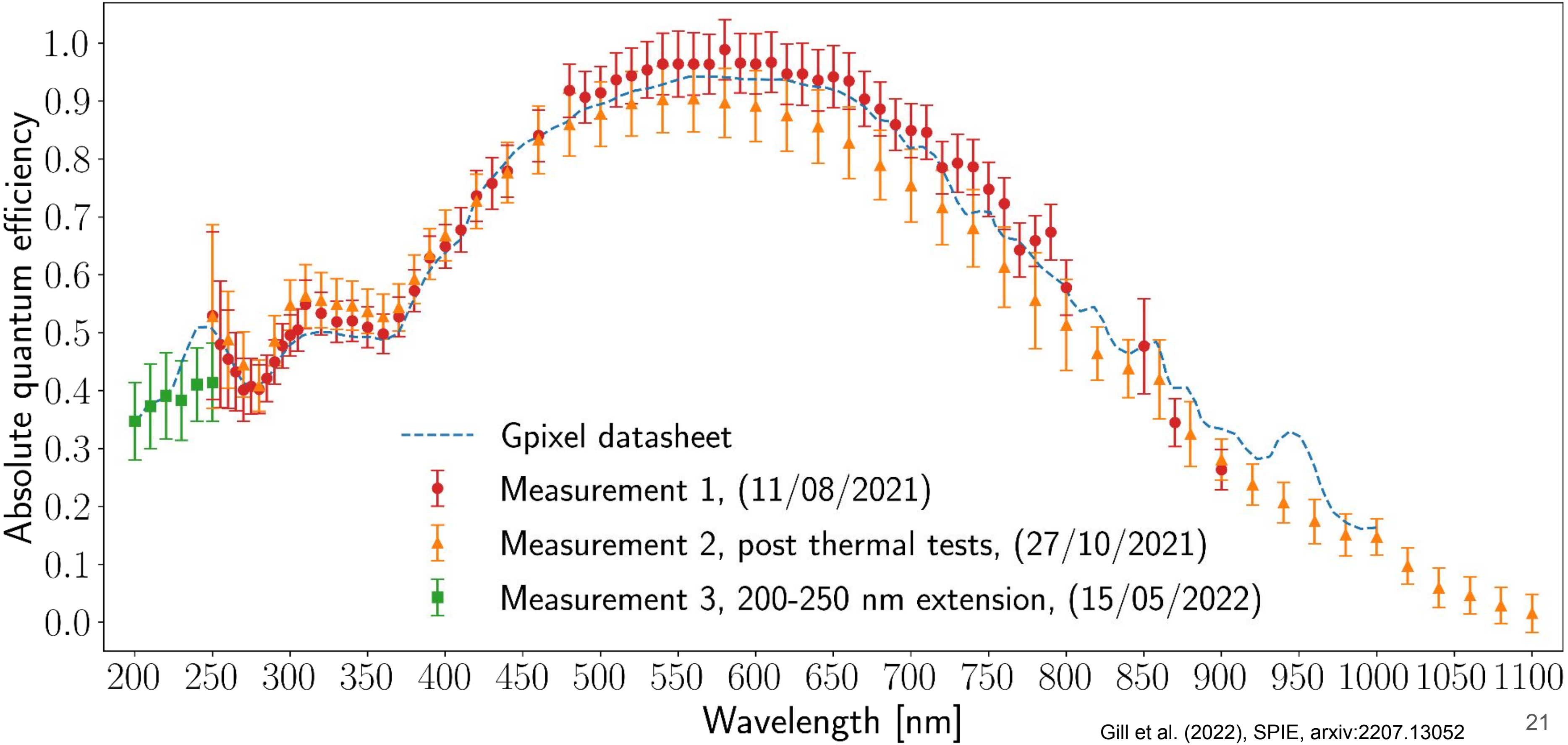

Gill et al. (2022), SPIE, arxiv:2207.13052

Sensor characterization: dark current

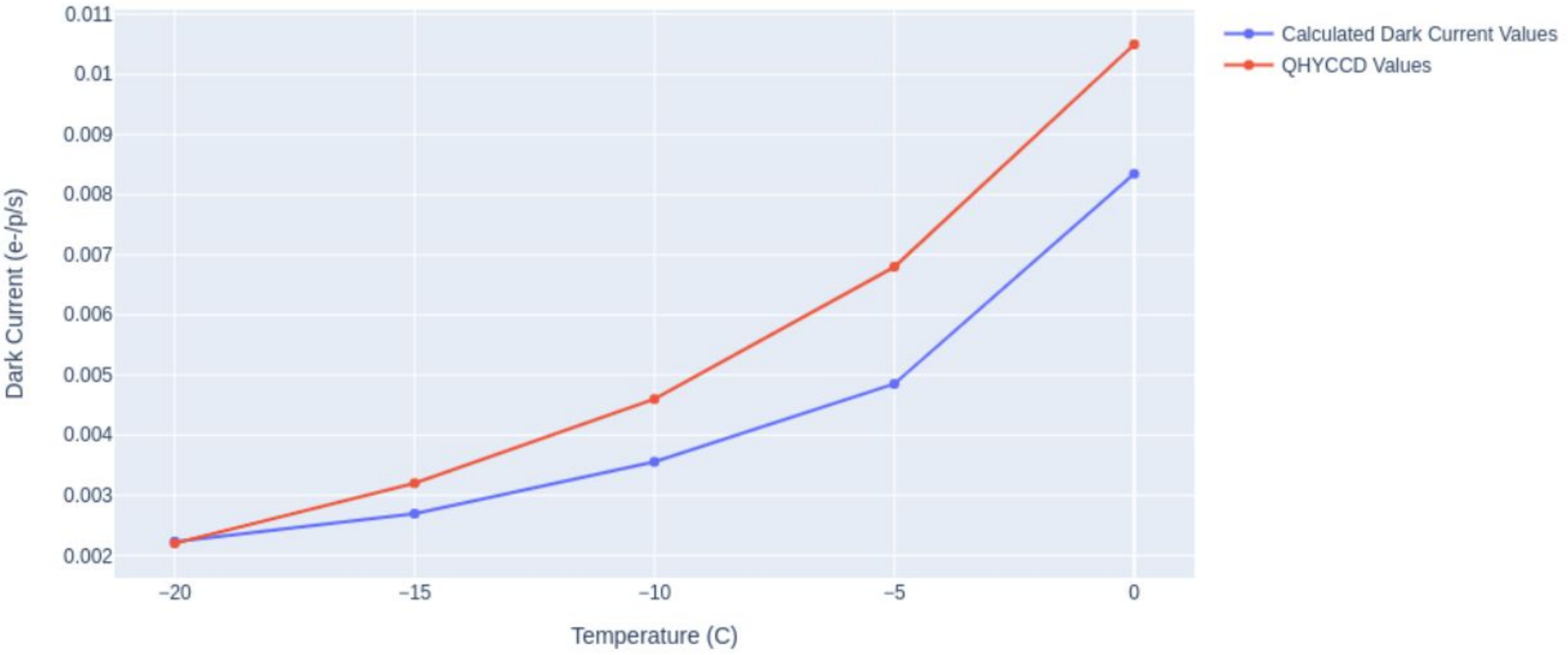

Credit: Emaad Paracha (MSc Thesis)

Filter transmission

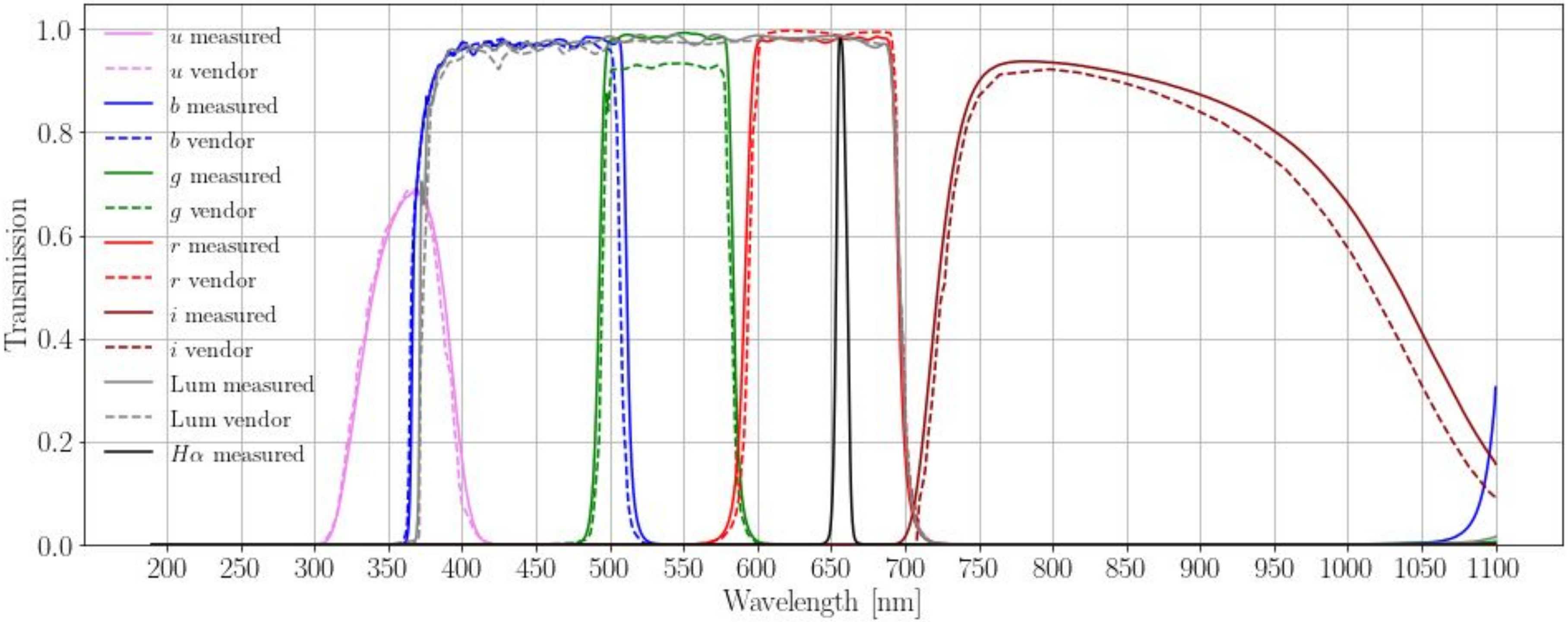

Bandpass estimates

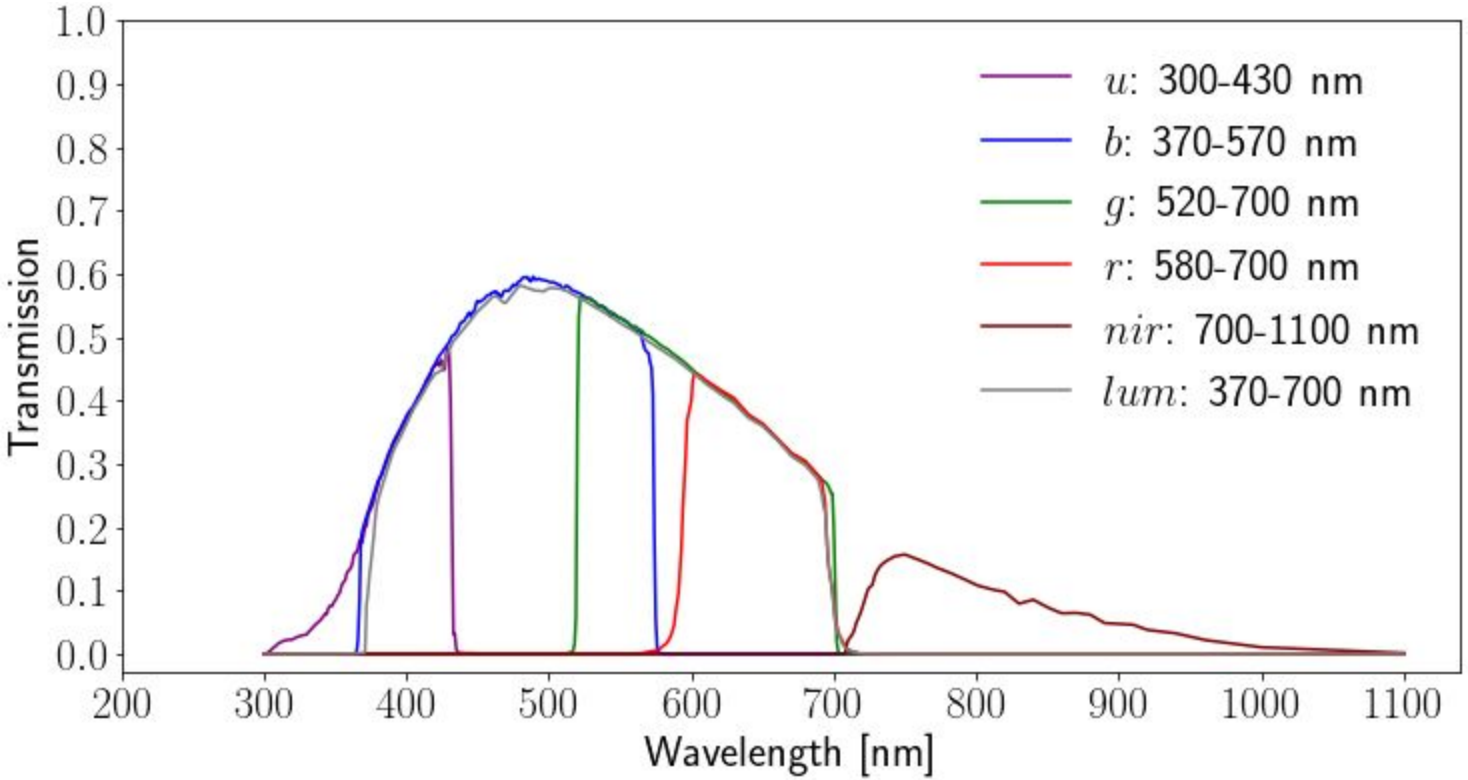

Exposure time and sensitivity

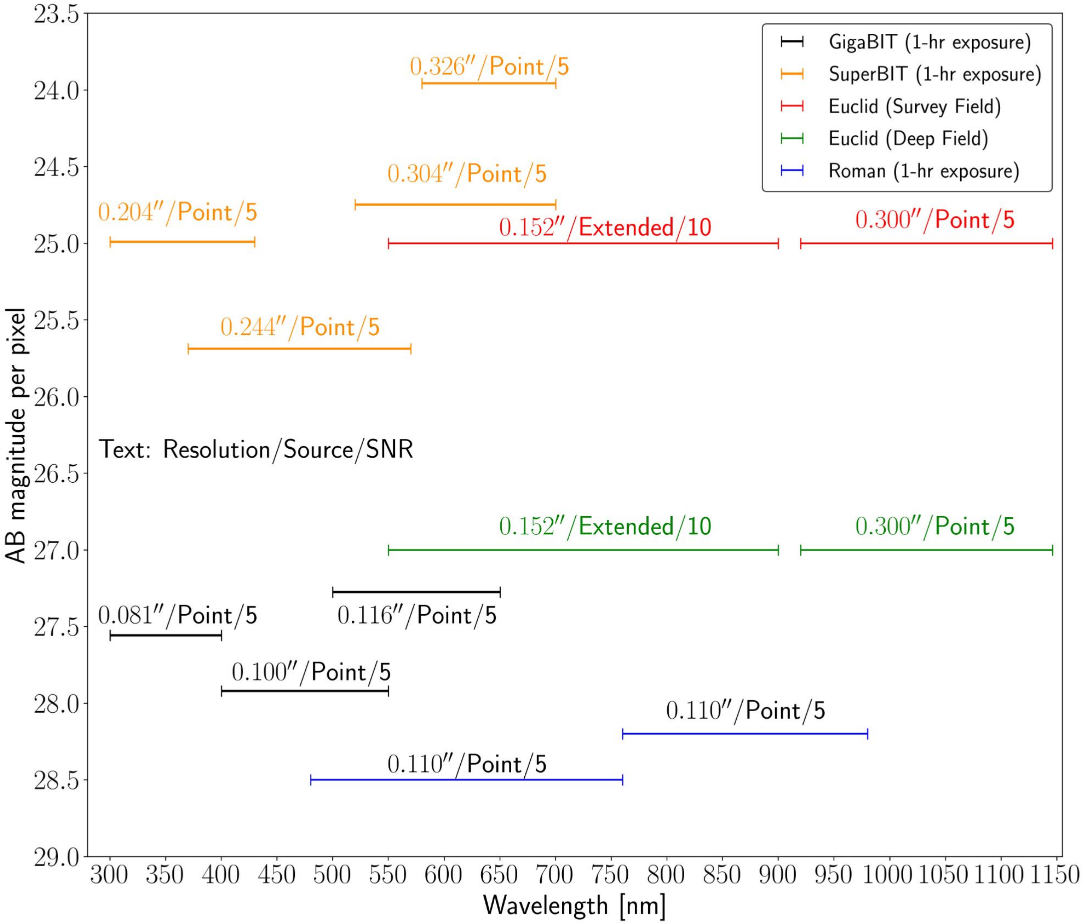

Galaxy number density forecasting

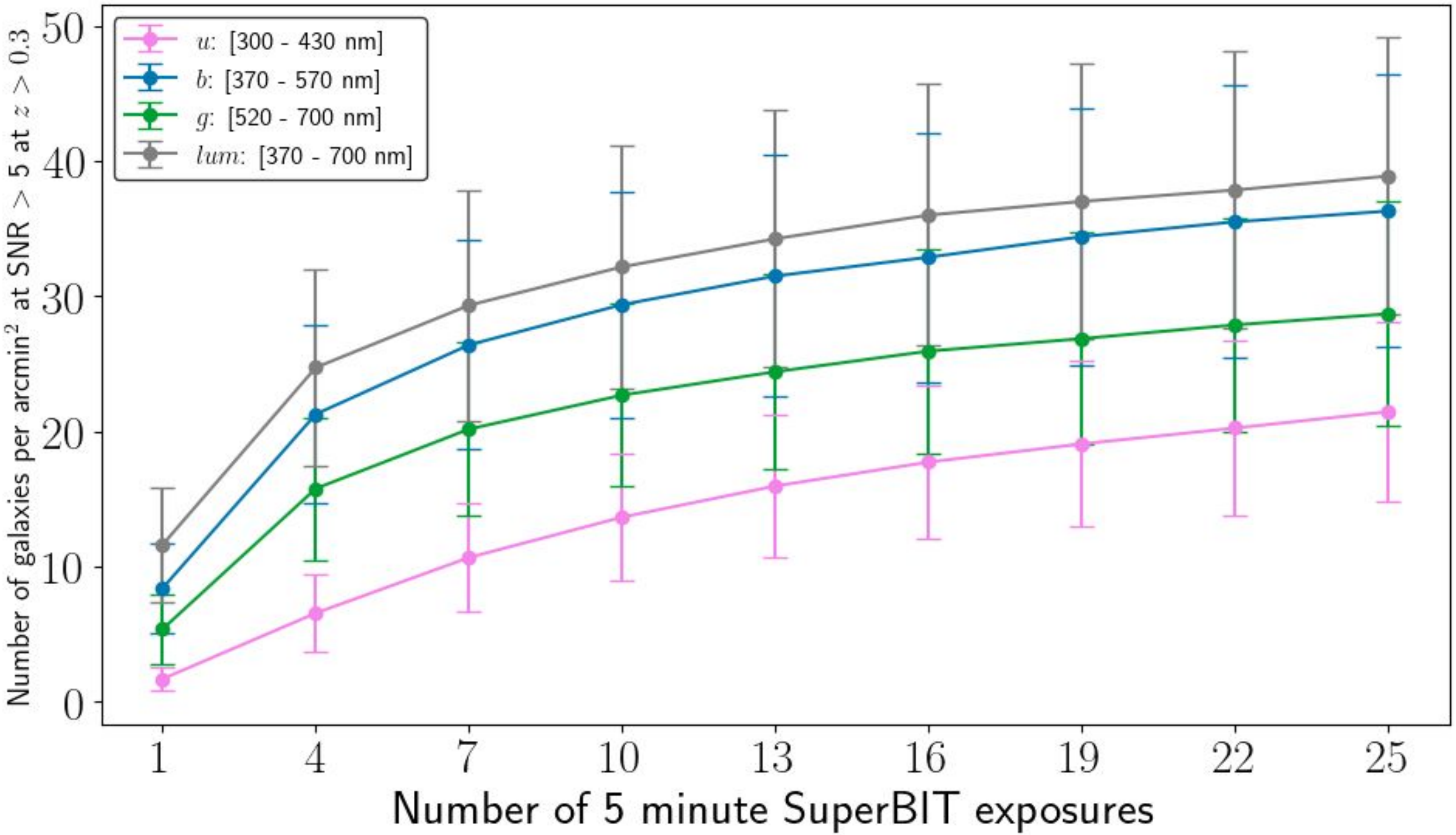

Wanaka campaign (Spring 2023)

Pointing and automation testing

Thermal

Communications

Optics cleaning

Data retrieval module testing

Debugging

Credit: NASA CSBF

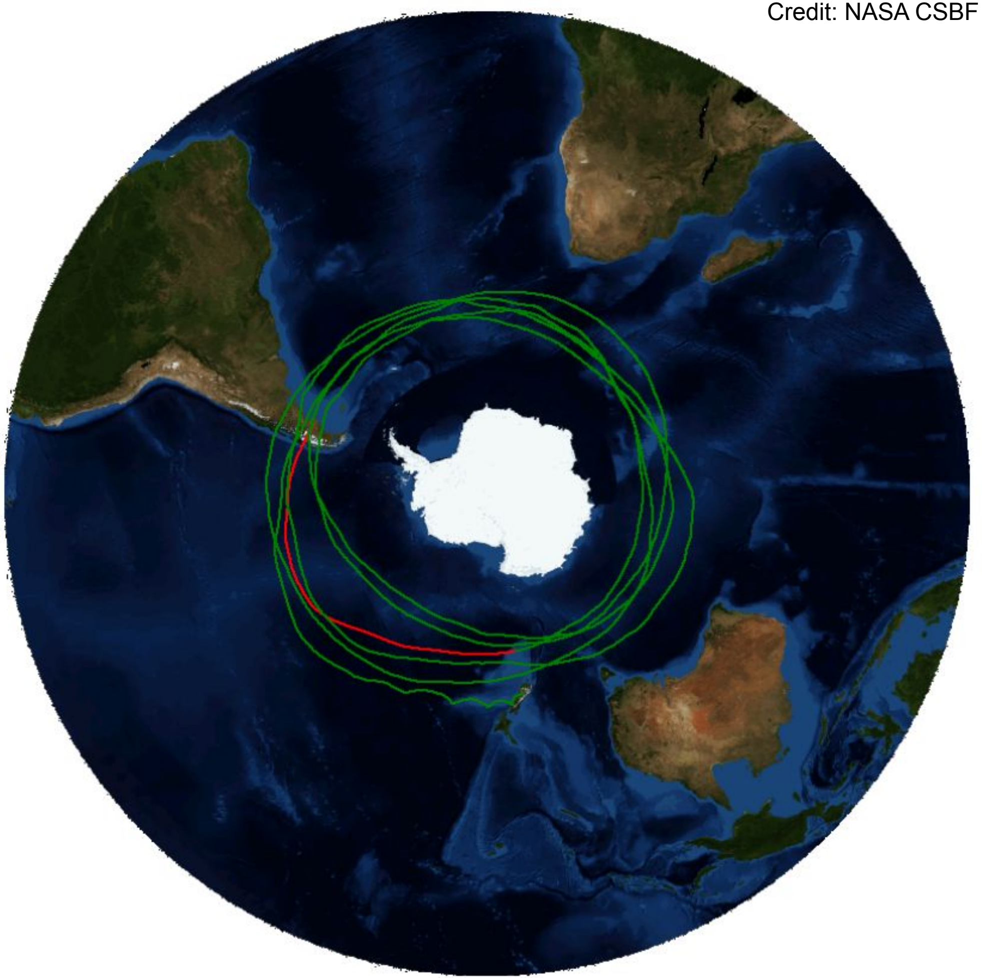

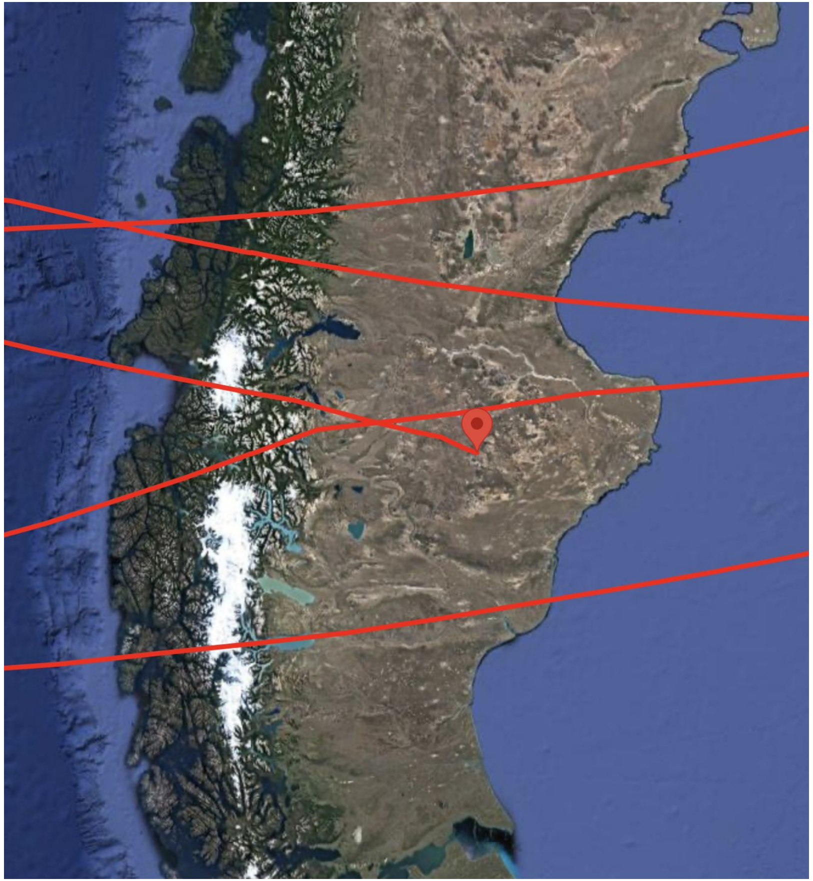

SuperBIT recovery

Pretty images

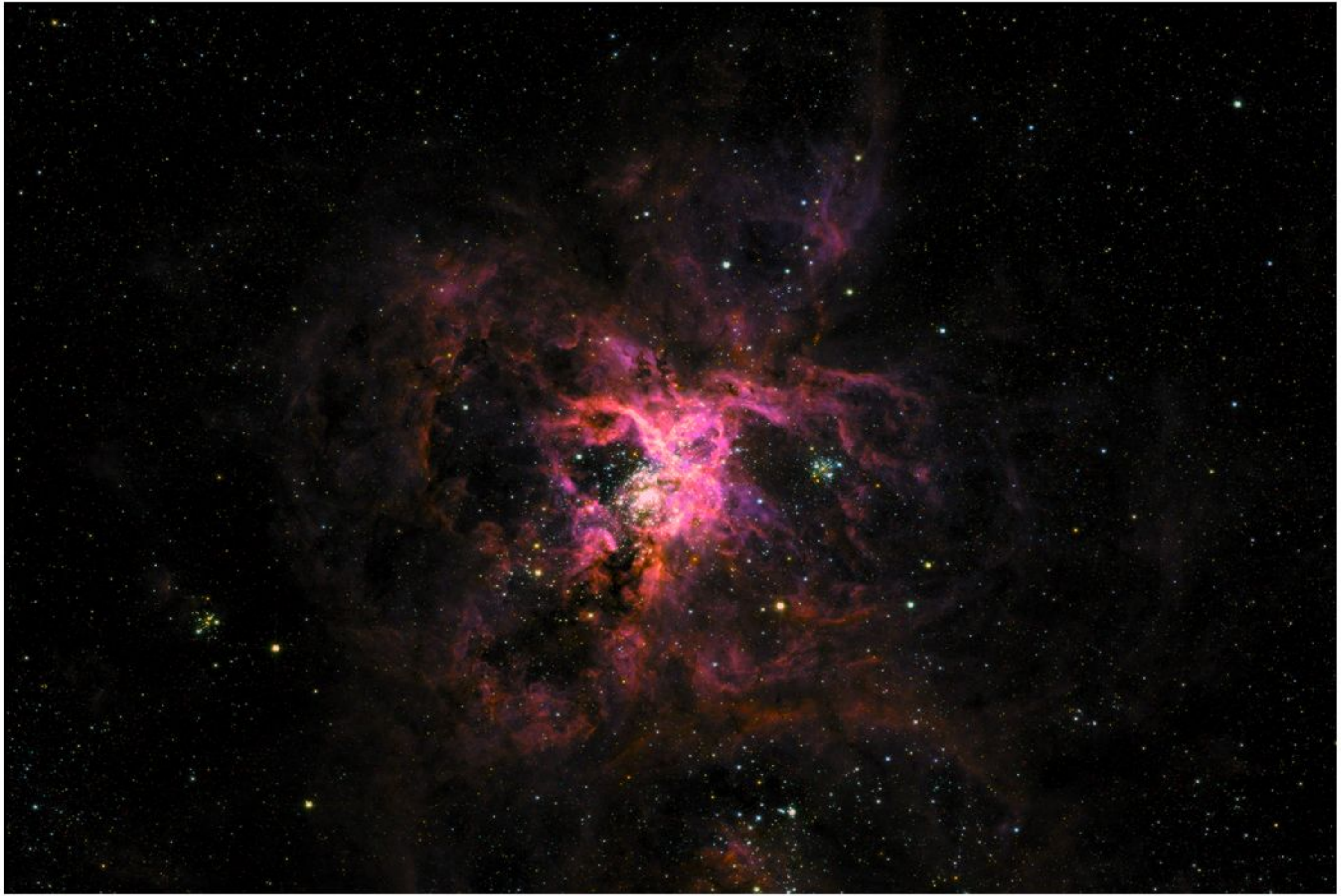

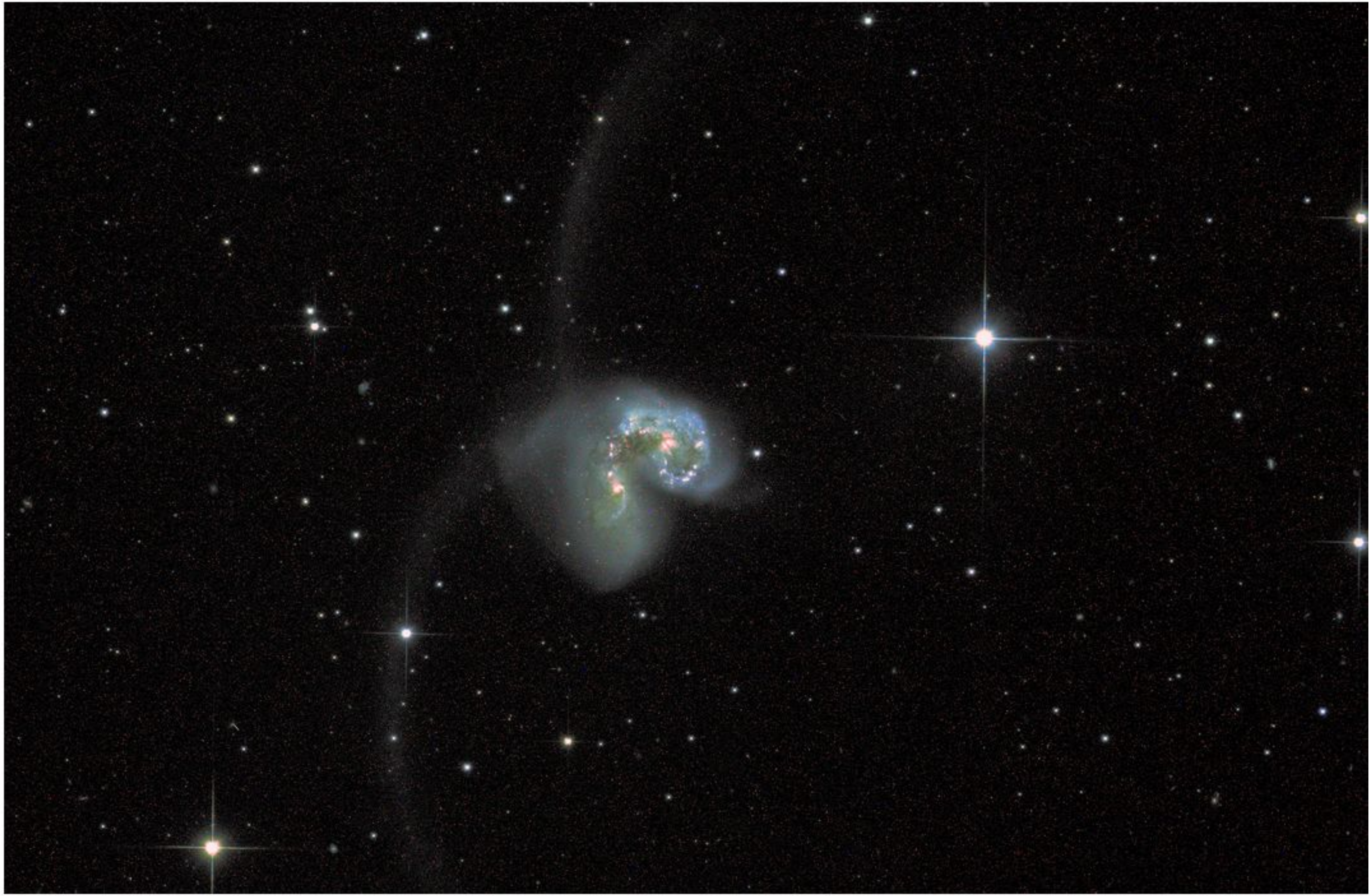

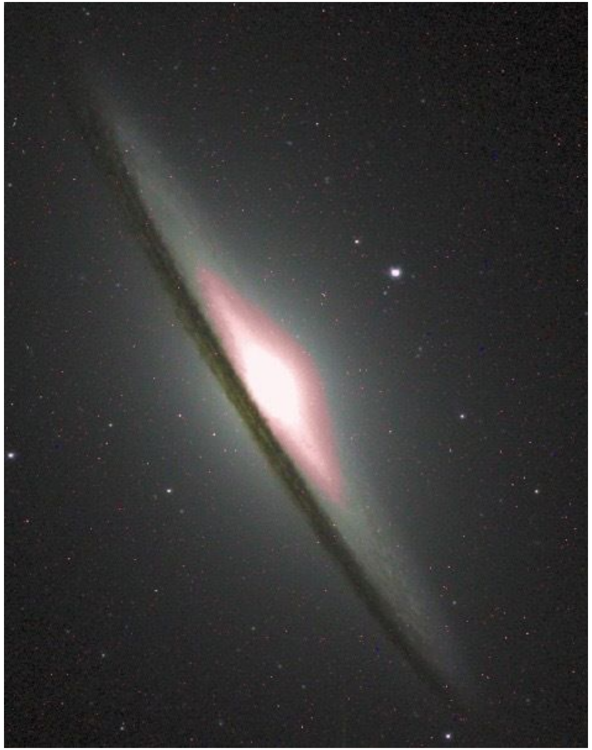


Bullet cluster
(zoomed out)

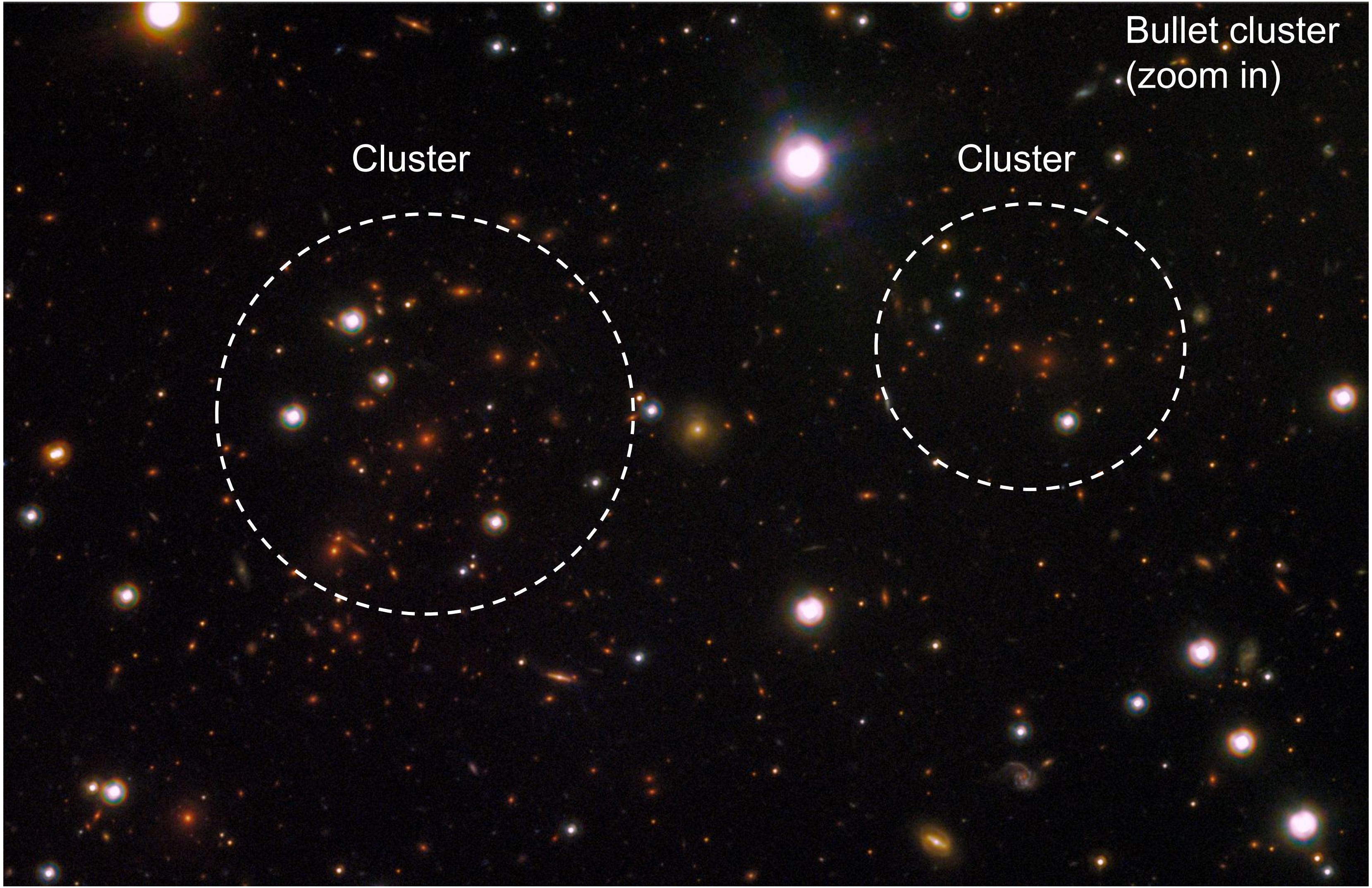
Bullet cluster
(zoom in)
Cluster
Cluster


Abell 1689
(zoomed out)

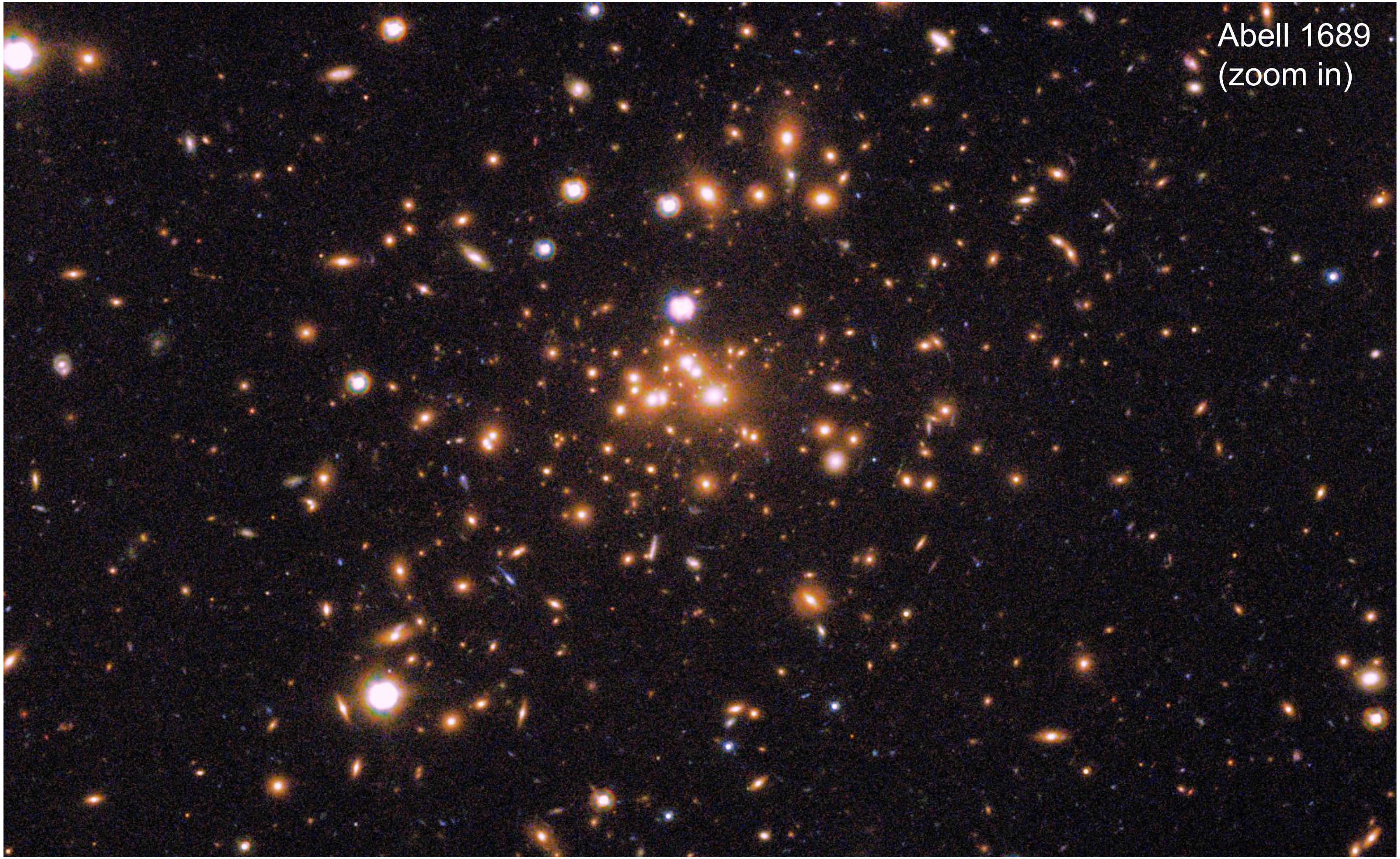
Abell 1689
(zoom in)


Abell 3827
(zoom out)

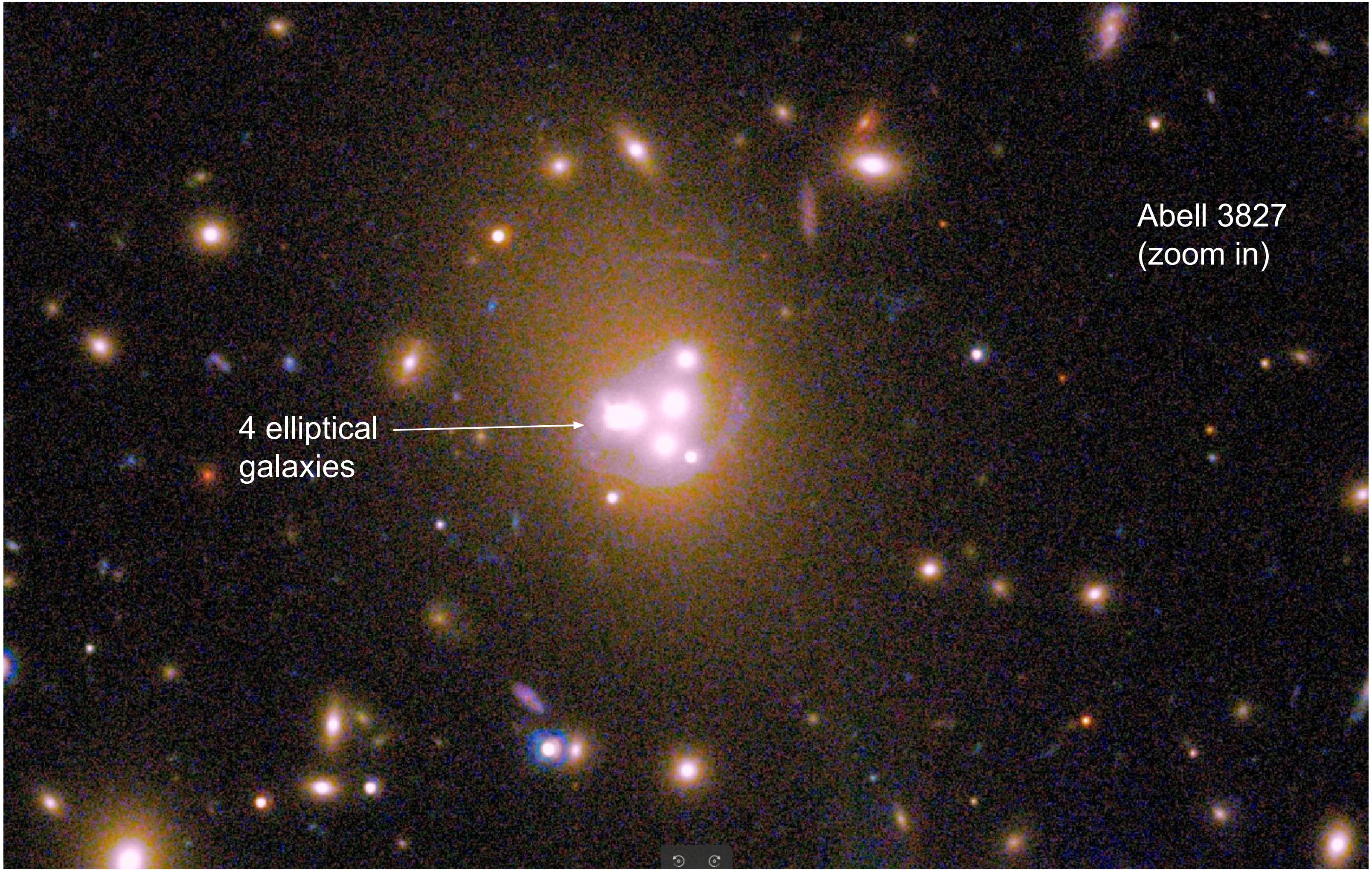
Abell 3827
(zoom in)
4 elliptical
galaxies

Preliminary results

Coarse telescope stability

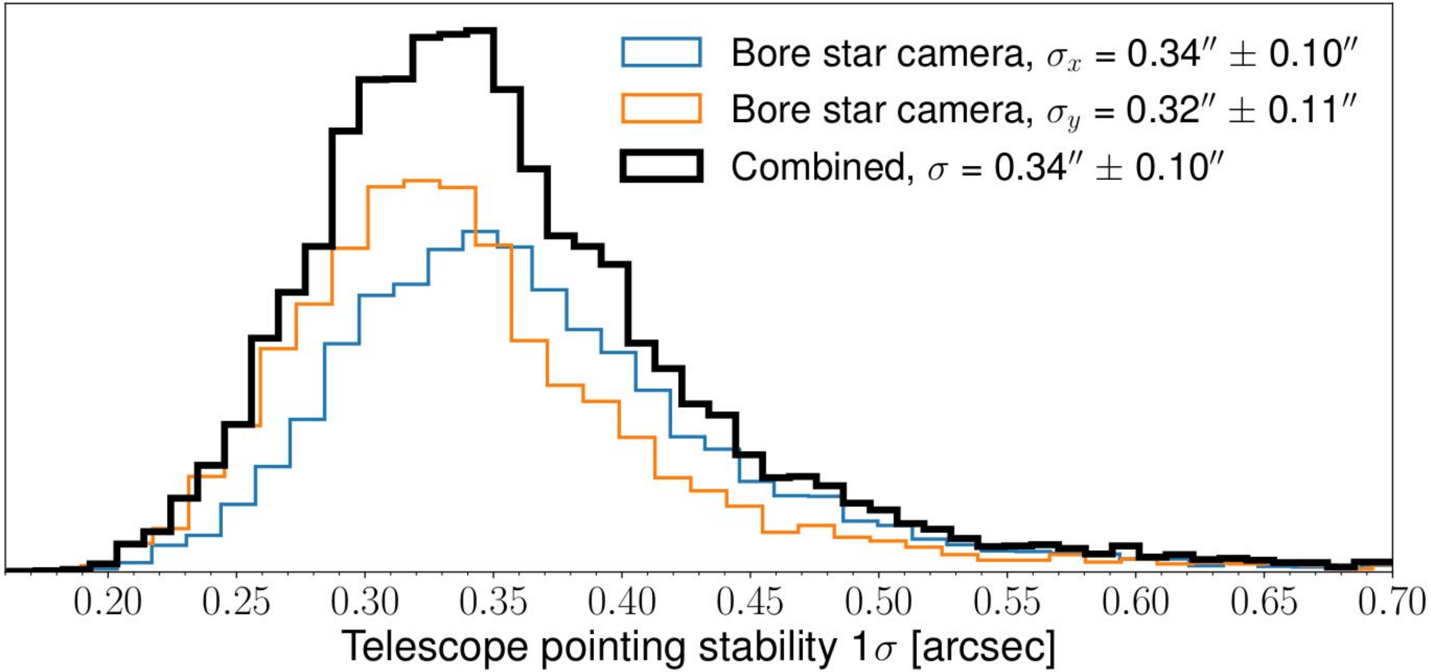

Gill et al. (2024) (submitted)

Focal plane stability

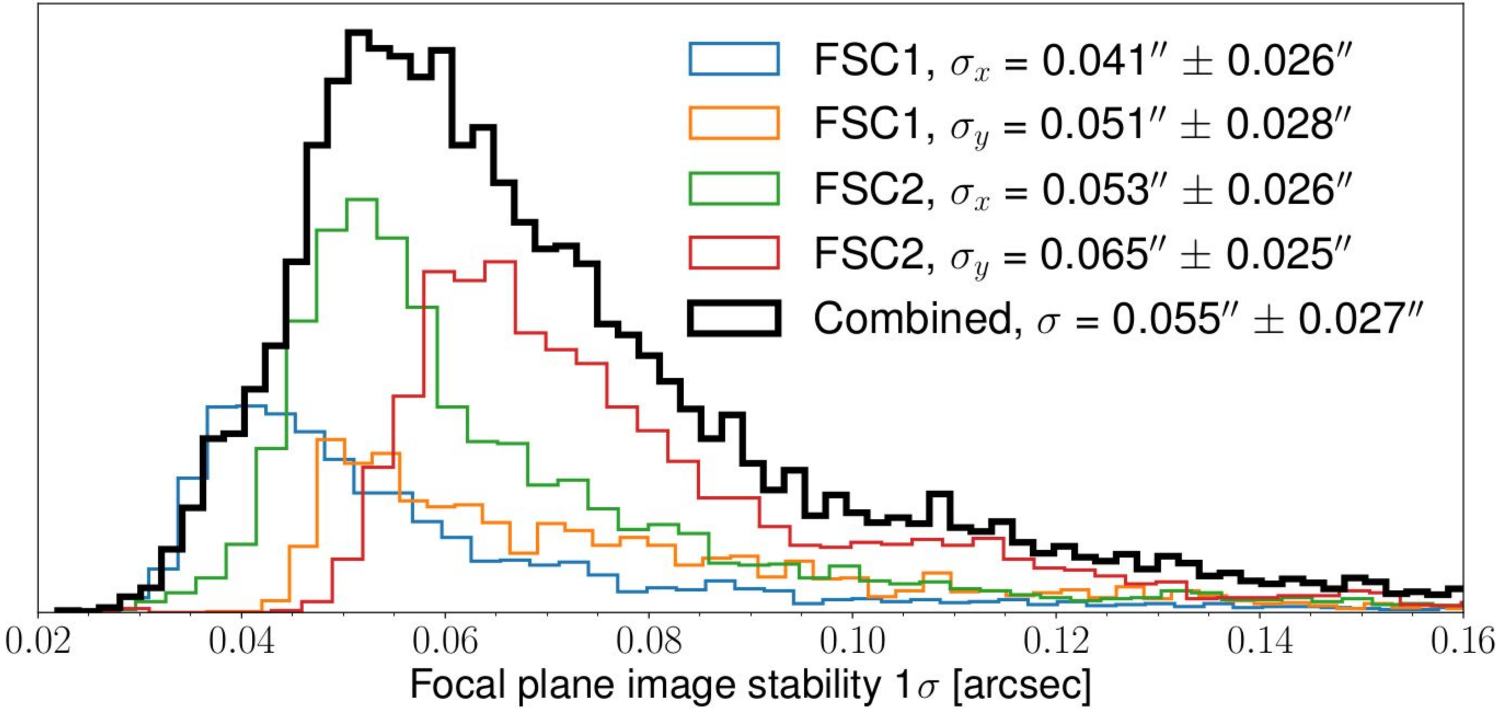

Gill et al. (2024) (submitted)

Point-spread function

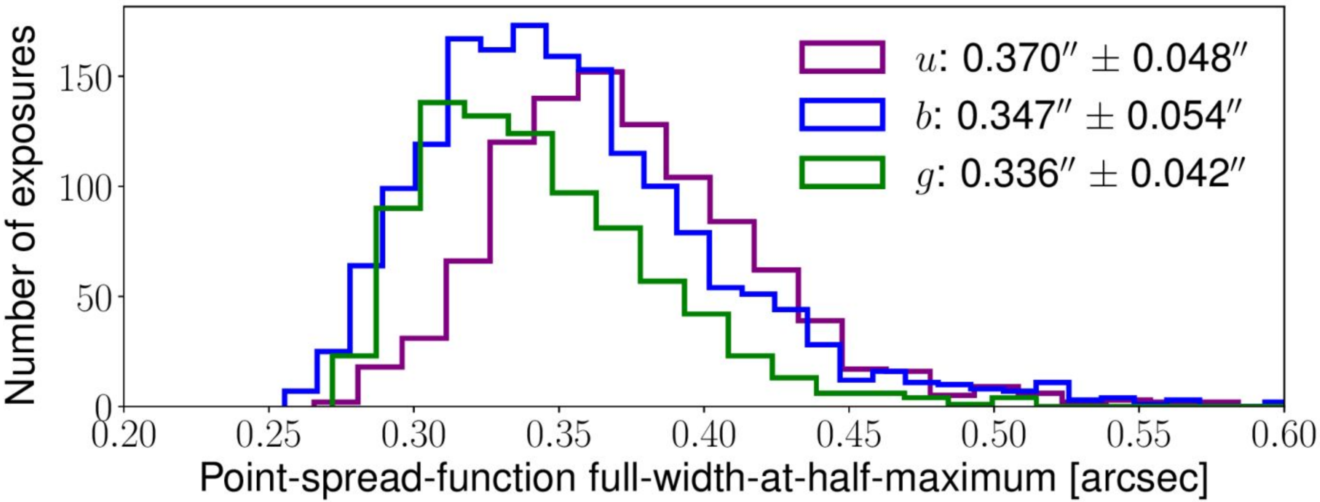

Gill et al. (2024) (submitted)

Point-spread function

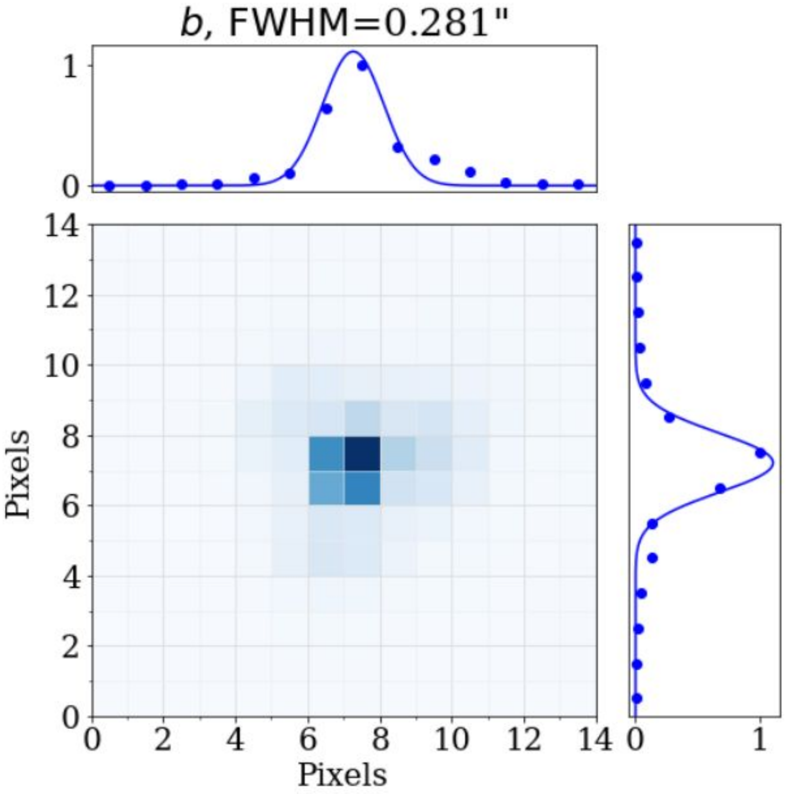

Ellipticity of stars and galaxies

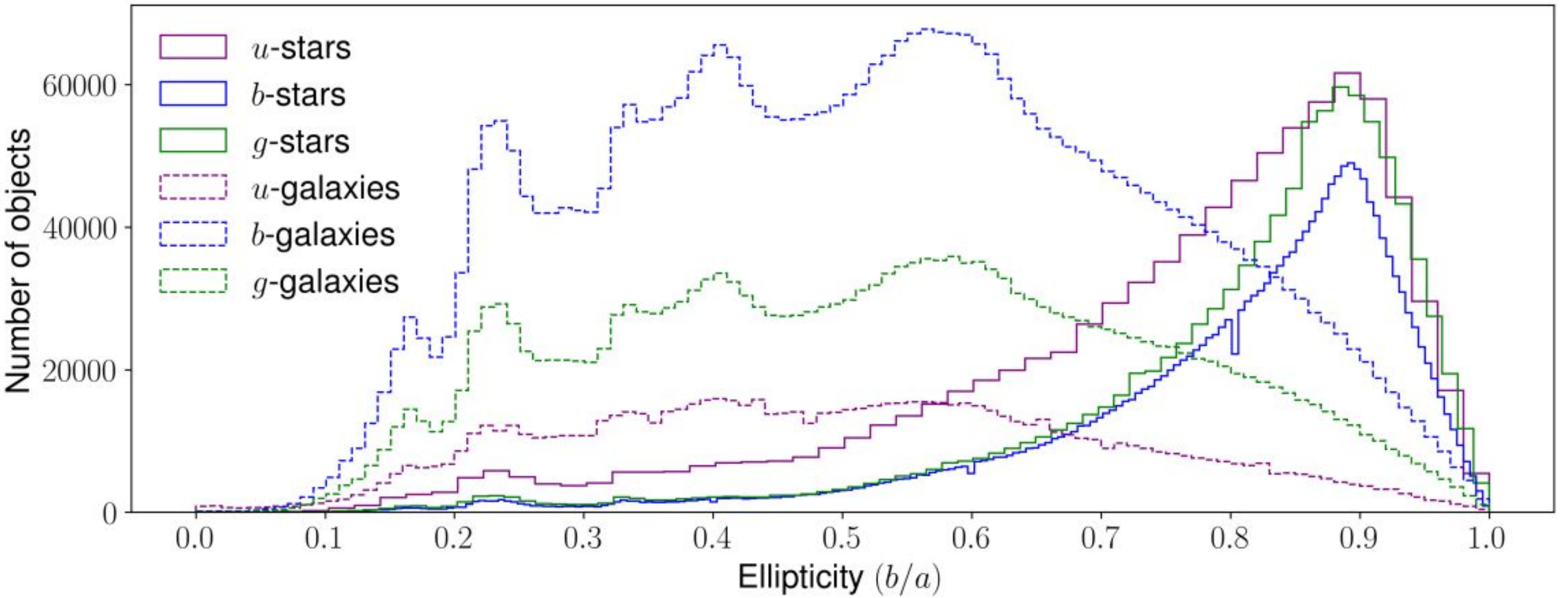

Size distribution of galaxies

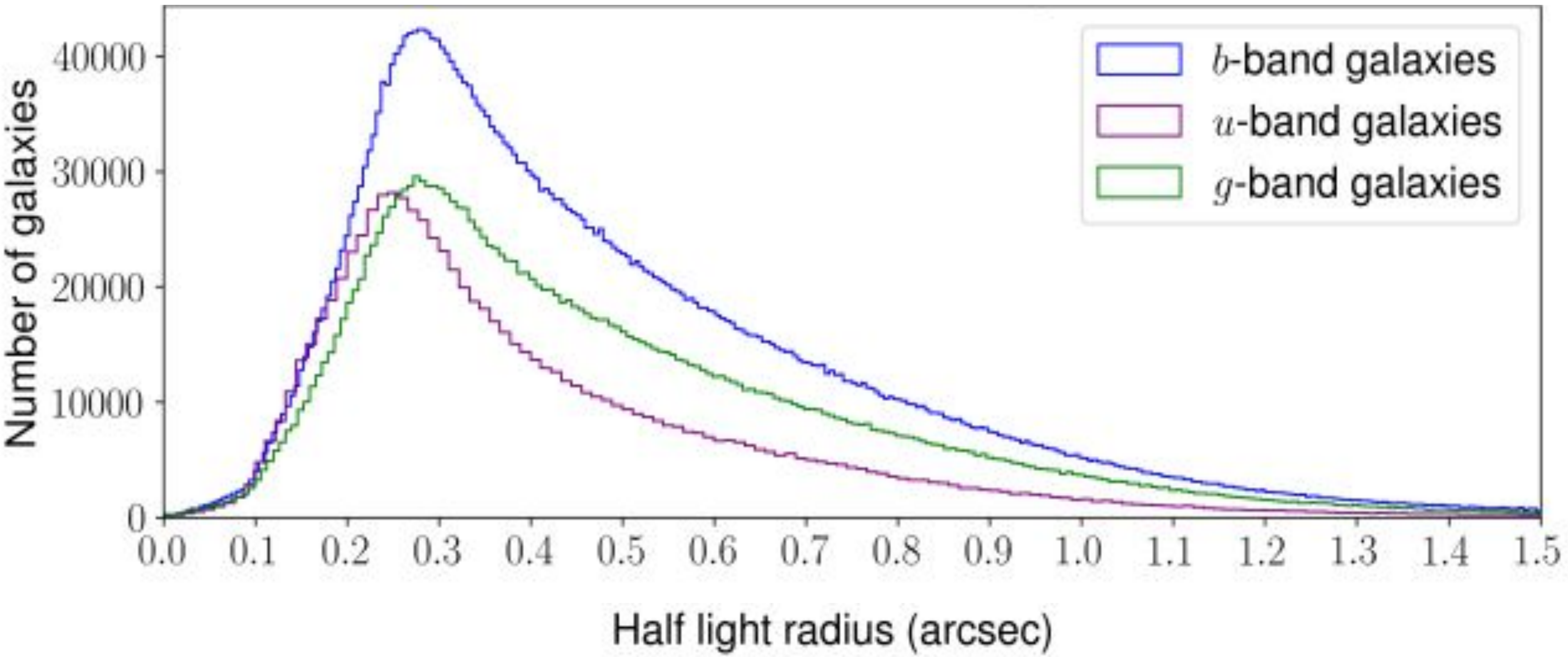

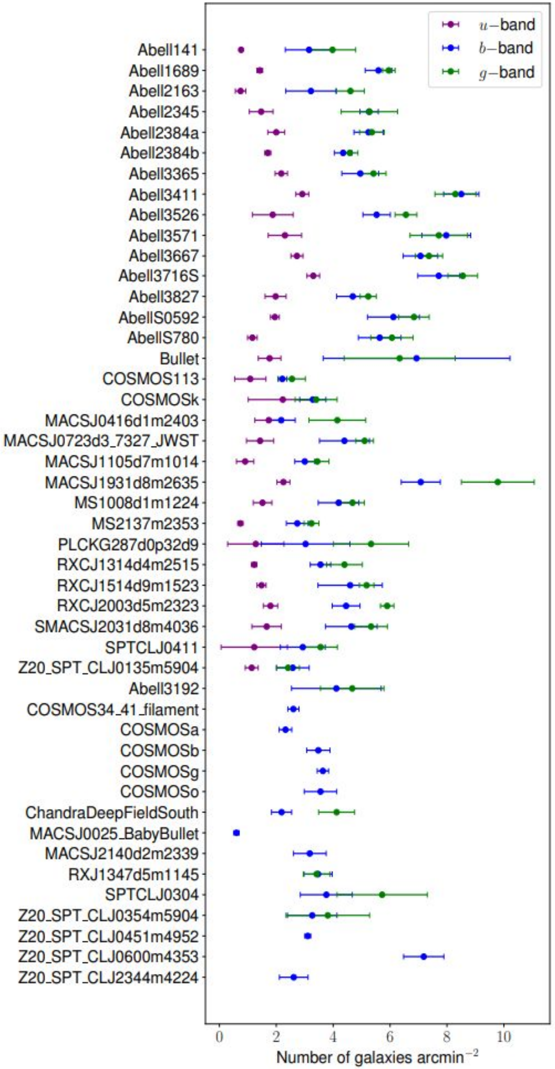

Number density of galaxies per arcmin^2 per individual image

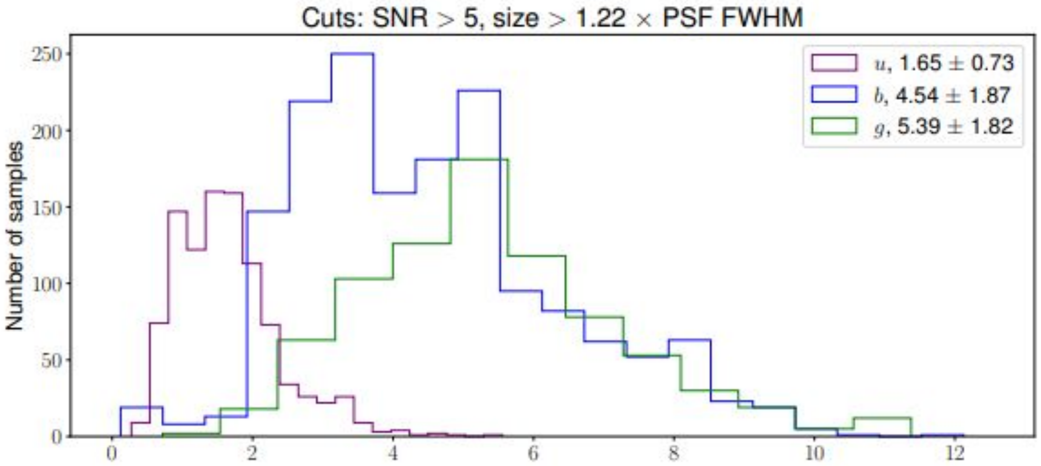

Pre-flight bandpass accuracy

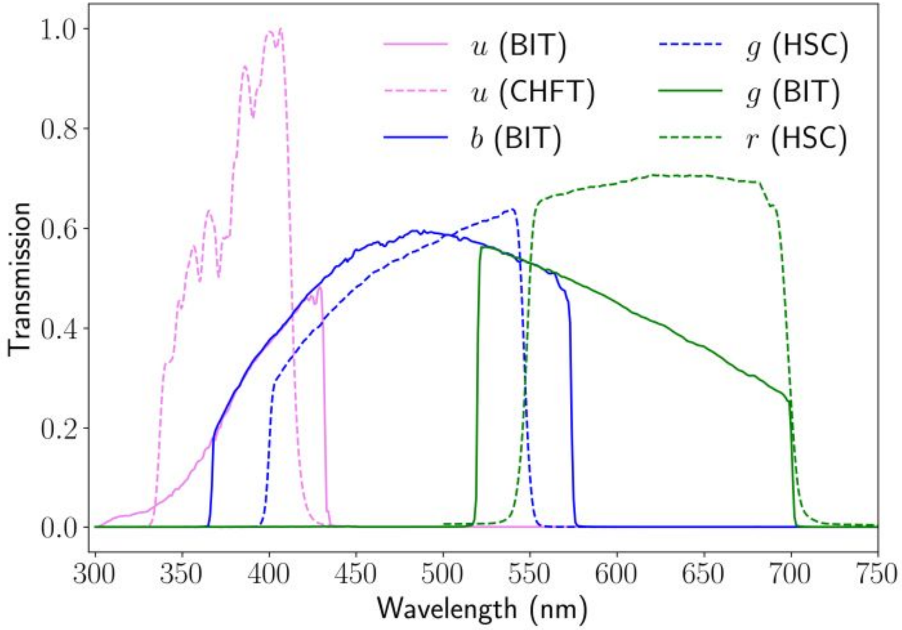

Pre-flight bandpass accuracy

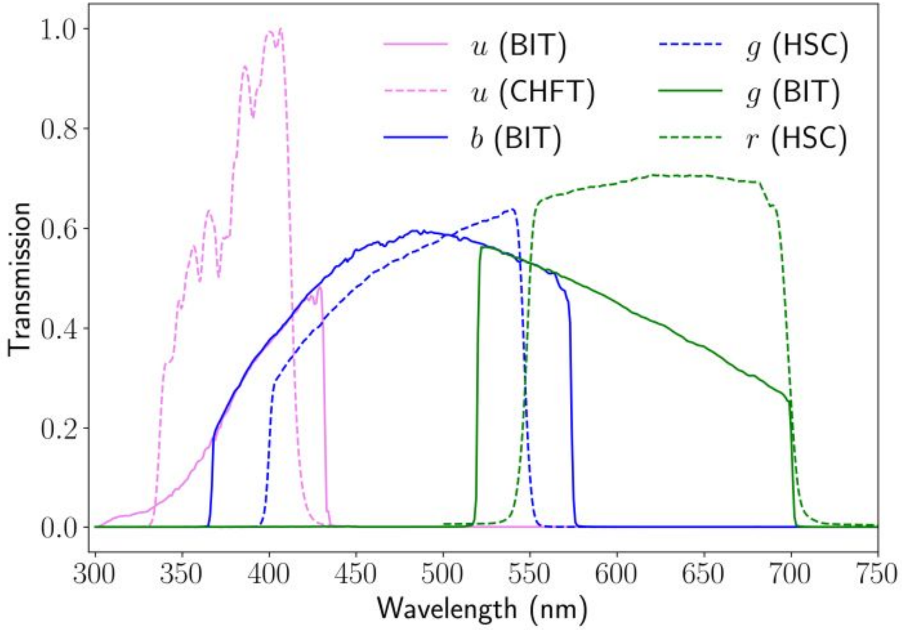

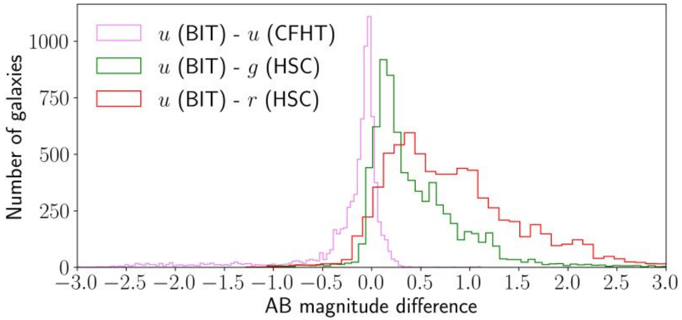

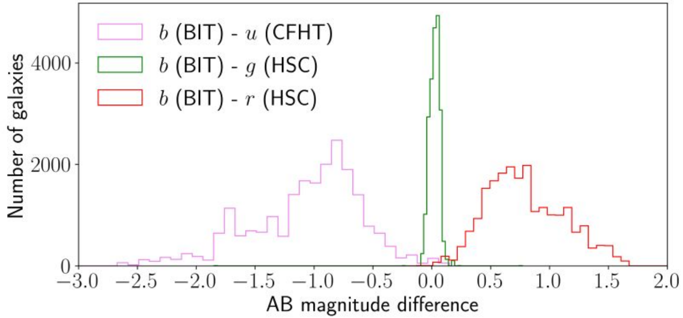

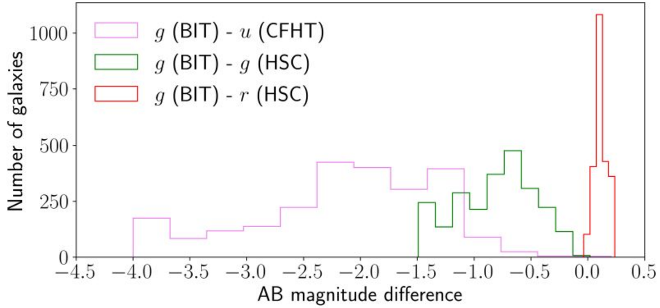

Sky background and impact on galaxy depth

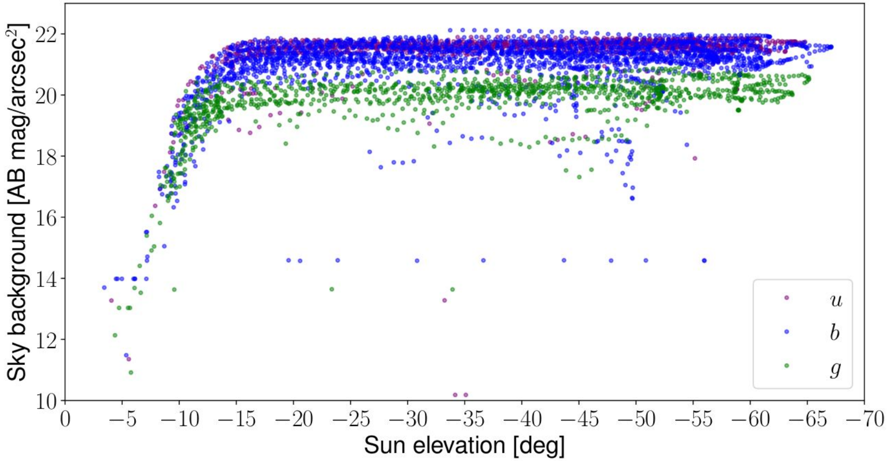

Sky background and impact on galaxy depth

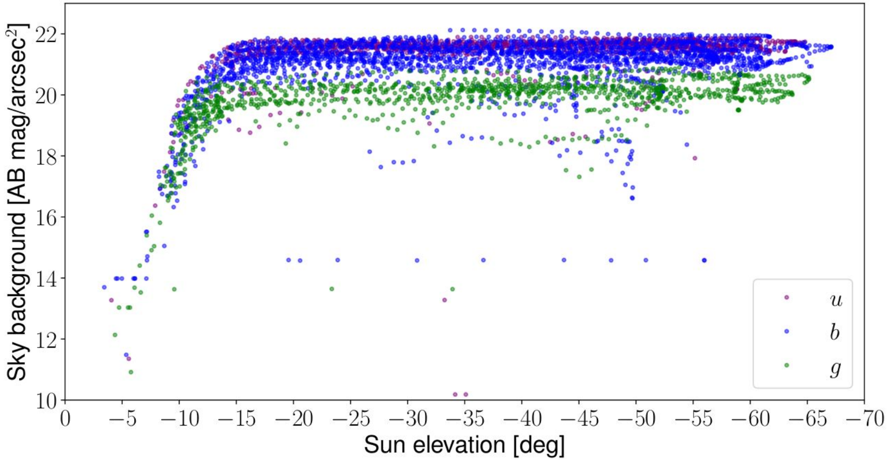

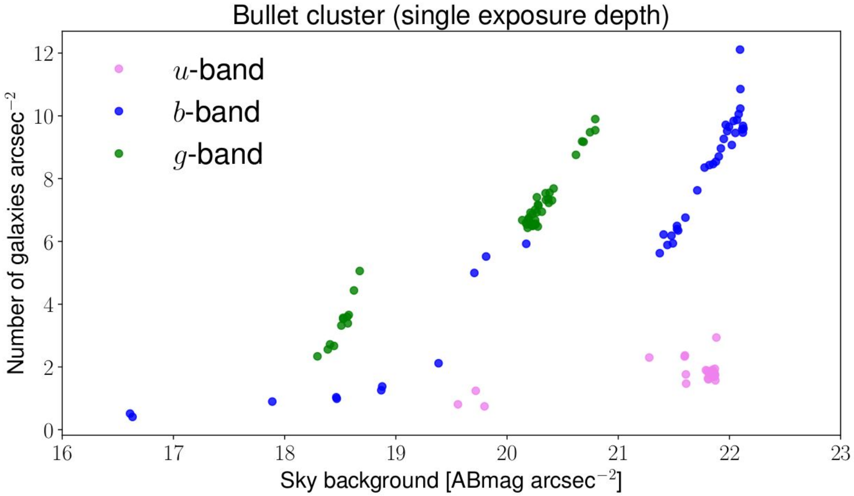

Challenges and learnings

- How do you determine that the previous image was "good"?
    - PSF size, ellipticity, sky background, FGS lock, astrometry
- Autonomous scheduling
- Hot pixels can cause lead to lost lock on star cameras
- Aurora can lead to extra background for balloon observations
- Astrometry can be hard to solve in crowded fields
- Absolute photometric calibration

Next steps

- Flat fields
- Sky background
- Time evolution
    - Absolute photometric stability, dark current, hot pixels
    - Optics (alignment, focus etc)
- Weak lensing shear measurement, dark matter distributions
- GigaBIT (1.5 meter balloon telescope)
- CubeSats / small satellites for astronomy in era of "New Space"

MIT AEROASTRO

Thank you for your time

Extra slides

Parameter	SuperBIT	GigaBIT	Euclid	Webb	HST
Band	0.3-1.1 um	0.3-1.1 um	550 nm to 2 um	0.6 - 28.5 um	0.2-1.7 um
Diameter (m)	0.5	1.34	1.2	6.5	2.4
Collecting area (m^2)	0.20	1.41	1	25	4
PSF size (")	0.35	0.1	0.15	0.065	0.07
Field of view (deg^2)	0.09	0.25	0.57	0.0026	0.003
Focal ratio	11	11	20	20	24

Band	λ_{p} **[nm]**	**Airy**	**Optics**	**Optics + jitter** $(0.05'', 1\sigma)$	**Measured**	**Difference** (σ)
u	395	$0.199''$	$0.252''$	$0.278''$	$0.370'' \pm 0.048''$	1.92
b	476	$0.240''$	$0.293''$	$0.315''$	$0.347'' \pm 0.054''$	0.59
g	597	$0.300''$	$0.337''$	$0.357''$	$0.336'' \pm 0.042''$	0.50

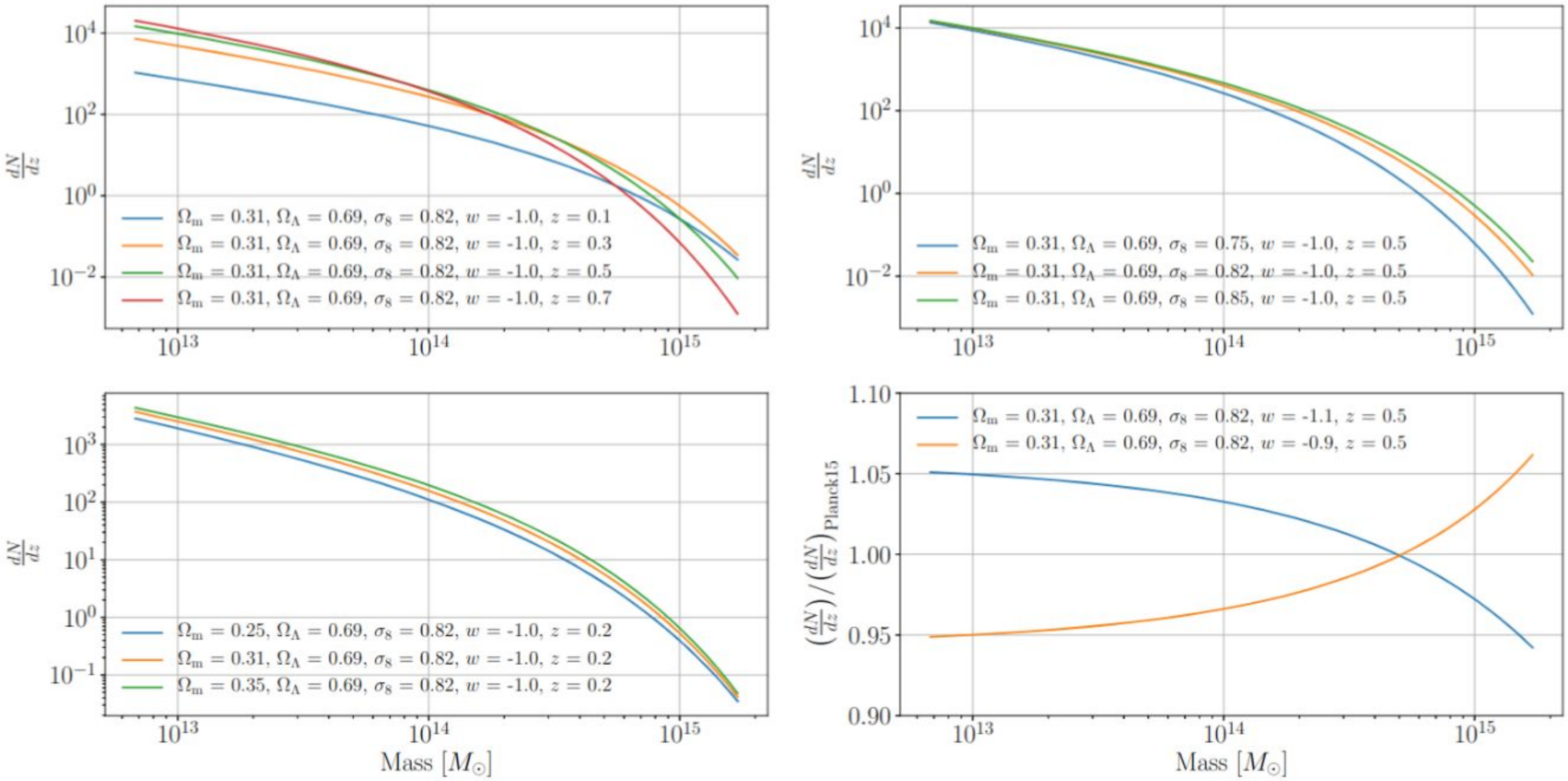

Figure 1.4: The number of clusters per unit redshift versus mass expected for a hypothetical 60 deg^2 survey.

Self-interacting dark matter

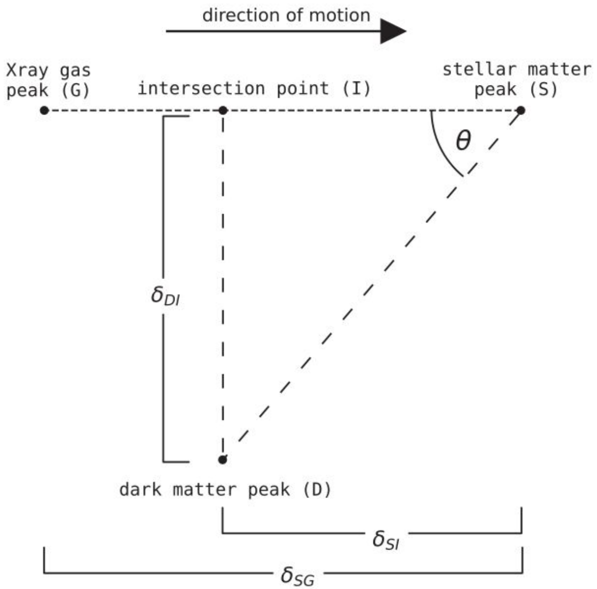

Figure 1. During a collision between galaxy clusters, the galaxies (S for 'stars'), gas (G), and dark matter (D) can become separated. The offset between each halo's stars and gas, $\delta_{\rm SG}$, indicates its approximate direction of motion, because of ram pressure on the gas. Relative to this direction of motion, we express the offset between stars and *dark matter* as parallel, $\delta_{\rm SI}$, and perpendicular, $\delta_{\rm DI}$ components.

$$\beta_{\parallel} \equiv \frac{\delta_{\rm SI}}{\delta_{\rm SG}}$$

$$\beta_{\perp} \equiv \frac{\delta_{\rm DI}}{\delta_{\rm SG}}$$

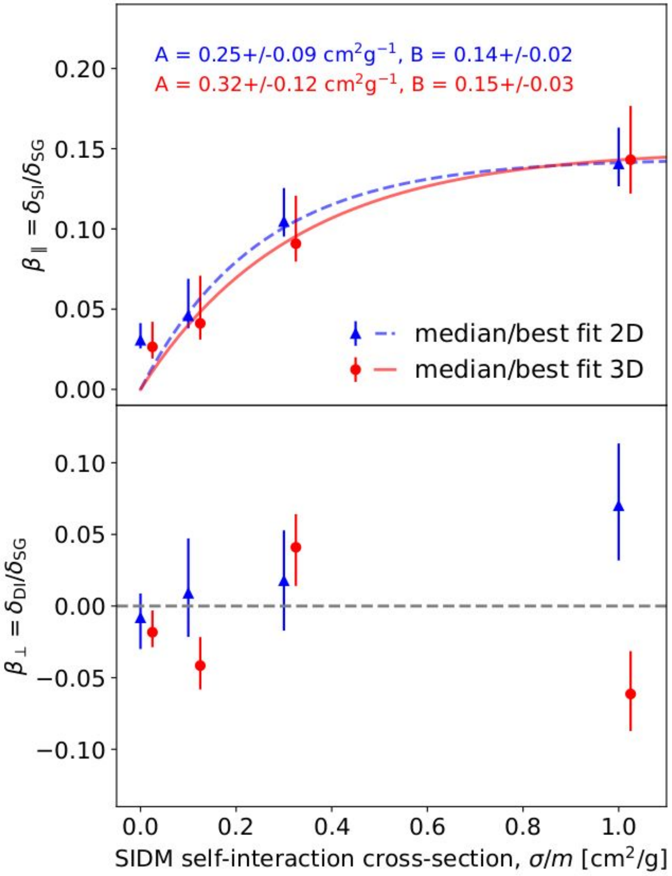

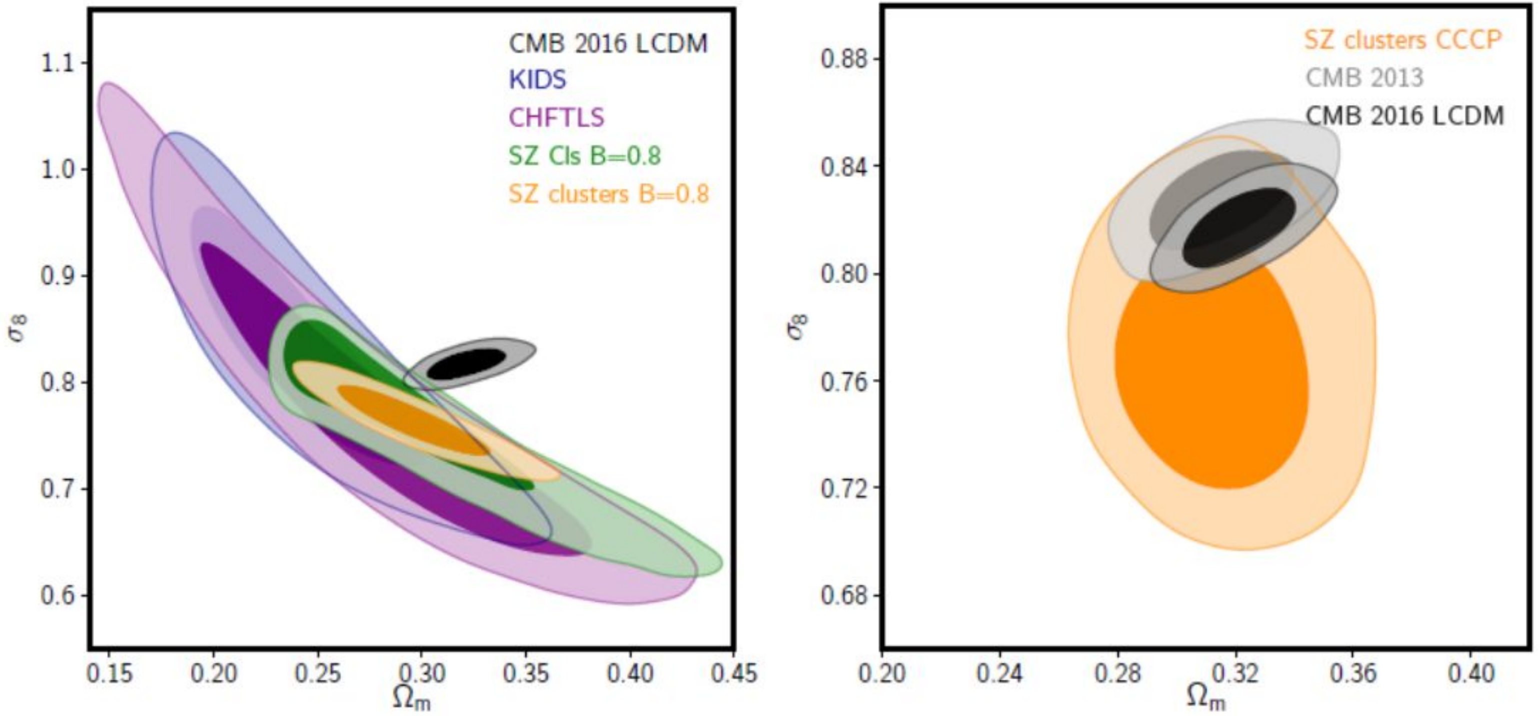

Figure 1.8: Left: Constraints on σ_8 and Ω_m from the large-scale structure compared with the CMB (black contours). Right: Comparison of SZ cluster count constraints from *Planck* (yellow) using the Canadian Cluster Comparison Project (CCCP) prior on the mass bias and *Planck* constraints from 2013 and 2016 (grey and black). The variation in τ between the *Planck* releases is the primary cause of the difference in constraints from the CMB (Douspis et al., 2019).